9698 *Macromolecules* **2010**, *43*, 9698–9713
DOI: 10.1021/ma1017132

Macromolecules
ARTICLE

Pyridine−EDOT Heteroarylene−Vinylene Donor−Acceptor Polymers[⊥]

Alessandro Abbotto,*,[†] Erika Herrera Calderon,[†] Milind S. Dangate,[†] Filippo De Angelis,[‡] Norberto Manfredi,[†] Claudio Maria Mari,[†] Chiara Marinzi,[†] Edoardo Mosconi,[‡] Michele Muccini,[§] Riccardo Ruffo,[†] and Mirko Seri[§]

[†]*Department of Materials Science and Solar Energy Research Center (MIB-SOLAR), University of Milano-Bicocca, Via Cozzi 53, I-20125, Milano, Italy,* [‡]*Istituto CNR di Scienze e Tecnologie Molecolari (CNR-ISTM) and Dipartimento di Chimica, Università di Perugia, Via Elce di Sotto 8, I-06123, Perugia, Italy, and* [§]*Consiglio Nazionale delle Ricerche, Istituto per lo Studio dei Materiali Nanostrutturati (CNR-ISMN), Via P. Gobetti 101, I-40129 Bologna, Italy*

Received July 29, 2010; Revised Manuscript Received October 22, 2010

ABSTRACT: Two heteroarylene-vinylene donor−acceptor polymers, **P(2,6-Py-V-EDOT)** and **P(2,5-Py-V-EDOT)**, containing vinylene-spaced simple donor (EDOT) and acceptor (pyridine) moieties, are presented. The central pyridine ring of the repeating unit is either 2,6- or 2,5-substituted, leading to different structural and electronic properties of the monomers. Polymers were obtained by either oxidative electropolymerization or Yamamoto coupling and fully characterized by NMR, UV−vis absorption, GPC, TGA, DSC, electrochemistry, and spectroelectrochemistry. Detailed ab initio computations have been performed for the monomers and model oligomers for analyzing their optical and electronic properties. GPC showed that isolated polymers obtained via Yamamoto poly coupling have low molecular weights, likely due to solubility issues. The electrochemical polymerizations led to p- and n-dopable polymers, with **2,5-Py-V-EDOT** yielding more reversible n-doped process. The energetic positions revealed HOMO (−5.1 and −5.0 eV), LUMO (−3.4 eV), and narrow bandgap (1.6 and 1.7 eV) energies closely matching materials-design rules for optimized organic photovoltaic devices. Preliminary investigation in photovoltaic devices in combination with C_{71}−PCBM afforded relatively modest power conversion efficiencies of ∼0.5% (AM 1.5G, 100 mW/cm^2), which were attributed to the low molecular-weight of the polymers accessible via the chemical route.

Introduction

Low-bandgap polymers have recently received considerable interest for their applications in organic electronics and optoelectronics,[1] including photovoltaics,[2,3] electrochromics,[4,5] and field-effect transistors.[6] It is now apparent that a successful design strategy to obtain narrow bandgap conjugated polymers is represented by the donor−acceptor concept,[7] where alternating donor electron-rich (D) and acceptor electron-poor (A) fragments are combined in the polymeric backbone to form a conjugated D−A copolymer.[3,8−10] In D−A systems the low-bandgap feature originates from the fact that strong D groups raise the highest occupied molecular orbital (HOMO) level and A groups lower the lowest unoccupied molecular orbital (LUMO) level, making oxidation and reduction easier, respectively. The proper choice of D and A groups and their combination together with π-spacers of different nature afford tunable optical, electrochemical, and photovoltaic properties over a wide range.[11]

In the effort of pursuing new performing systems a variety of D and A groups have been so far proposed including highly sophisticated species. Curiously, some of most simple efficient D and A moieties have not received much interest. A significant number of the reported examples have relied on the donor capacities of electron-rich thiophene derivatives, including 3,4-ethylenedioxythiophene (EDOT).[8,9,12] Poly(3,4-ethylenedioxythiophene) (PEDOT) has a number of interesting properties for practical applications, such as high stability and conductivity of the oxidized form[12] and a suitable low-bandgap of 1.7 eV for use as a donor polymer in photovoltaic cells.[8c] Furthermore, the EDOT ring is known to give efficient electropolymerization.[12] As far as A groups are concerned, the use of the π-deficient pyridine ring (Py) as an acceptor has been restricted to very few examples,[8] including EDOT−Py[8b−d] or EDOT−bipyridine[10a,b] based polymers, despite the fact pyridine is the parent system of the vast class of the heteroaromatic π-deficient rings (azines).[13] In addition, the electronwithdrawing capacity of pyridine is highly ranked,[13,14] and its properties have been extensively exploited in molecular materials for many technological fields, such as nonlinear optics.[15,16] Finally, vinylene(V)-spaced D−A low-bandgap copolymers attracted our attention because of their very limited investigation[9] in comparison to their counterparts with direct D−A aromatic ring linkage. Swager, Epstein and co-workers have developed vinylene-linked donor−acceptor polymers with alkoxybenzene rings as donors and 2,5-pyridine moieties as an acceptor, pioneering the use of nitrogen-based aromatic ring as alternatives of conventional poly(*p*-phenylenevinylene) (PPV) systems.[17] During the progress of the present work a report was published on vinylene-linked D−A polymers in which Reynolds and co-workers pointed out the fact that this class of polymers is still largely unexplored because of the synthetic challenges.[9d] Indeed, we believe that vinylene-linked conjugated polymers might carry a series of relevant advantages over the more conventional systems, including planarization between adjacent aromatic units and ethenylic spacers, extended π-conjugation, efficient delocalization, and, accordingly, reduced bandgaps and enhanced optical properties in the low-energy spectral region.

Organic photovoltaics (OPV) based on polymer-fullerene bulk-heterojunction (BHJ) cells have attracted increasing attention in the scientific community during the past few years for its

[⊥] Dedicated to Professor Francesco Naso on the occasion of his 73rd birthday.

*Corresponding author. E-mail: alessandro.abbotto@mater.unimib.it.

 Published on Web 11/10/2010

Scheme 1. Type I and Type II D−A−D Polymers Investigated in This Work[a]

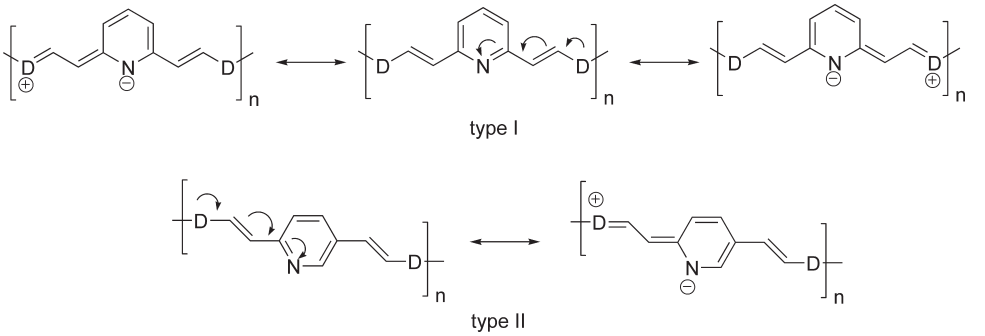

[a] Arrows indicate electron flow of the donor−acceptor behavior in the neutral polymers.

promise of a low-cost power source.[2] The BHJ cell is typically composed by an intimate blend between a p-type donor polymeric semiconductor and a n-type acceptor fullerene derivative such as C_{61}−PCBM ([6,6]-phenyl-C61-butyric acid methyl ester) or C_{71}−PCBM ([6,6]-phenyl-C71-butyric acid methyl ester).[18] The fundamental mechanism of a OPV cell is a 4-step process: (1) absorption of light by the polymeric semiconductor and generation of excitons (bound electron−hole pairs); (2) diffusion of excitons toward the polymer−fullerene interface; (3) dissociation of excitons at the interface due to the high electron affinity of the fullerene component and generation of free charge carriers; (4) transport and collection of charge carriers to their respective electrodes. Since only fullerene derivatives have been reported so far to give highly efficient OPV cells, the route for more performing devices goes through the optimization of the donor semiconducting polymer. The strategies to improve OPV power conversion efficiencies (PCEs) imply higher short-circuit current densities (J_{sc}), mainly by reducing the bandgap of polymers so as to harvest more sunlight, and higher open-circuit voltages (V_{oc}). Being V_{oc} proportional to the difference $LUMO_{PCBM} - HOMO_{polymer}$, this value can be increased by lowering the HOMO of the polymers.[19] Accordingly, the efficiency limitations of OPV cells have been recently discussed in terms of HOMO/LUMO and energy gap E_g energies.[19] Namely, material-design rules involve the following: (1) a $LUMO_{polymer}$ energy higher than that of the $LUMO_{PCBM}$, with an ideal minimal offset of 0.3 eV, which corresponds to a value of −4.0 eV (or higher) assuming −4.3 eV for $LUMO_{PCBM}$; (2) a bandgap in the range of 1.2−1.7 eV for efficient light harvesting extension to the low-energy portion of the solar emission; (3) accordingly, a $HOMO_{polymer}$ energy of ca. −5.2 to −5.7 eV. Recently, record efficiencies higher than 7% were achieved by using a donor low-bandgap polymer (PBDTTT−CF[20] or PTB7[21]) made of alternating electron-rich benzodithiophene and electron-poor thienothiophene fragments. For this polymer the HOMO, LUMO and bandgap energies were determined[21] to be −5.2, −3.3, and 1.8 eV, respectively, consistent with the above design rules.

On the basis of these premises we have decided to investigate the first examples of heteroarylene-vinylene D−A conjugated polymers where D is the electron-rich five-membered EDOT ring and A the six-membered pyridine ring. Polymers have been synthesized via oxidative electropolymerization and Yamamoto polymerization, and fully characterized in their optical, electrochemical, charge carrier mobility, and photovoltaic properties. DFT/TDDFT computations have been performed for the monomers and model oligomers for analyzing their optical and electronic properties. By using such design we demonstrate how it is possible to access new low-bandgap semiconducting polymers with tailored HOMO/LUMO and energy gap energies close to the design rules for efficient components in OPV.

Results and Discussion

Design of Polymers. We have designed two pyridylene−vinylene (Py−V) donor−acceptor copolymers: 2,6-pyridylene−vinylene polymers, where the central pyridine ring of the repeating unit is 2,6-substituted (type I), and 2,5-pyridylene−vinylene polymers, where the pyridine ring is 2,5-substituted (type II) by the two electron-rich fragments (Scheme 1). With respect to the central heteroaromatic ring the two donor-vinylene moieties are in *meta* and *para* position in type I and II polymers, respectively. Therefore, only type II polymers have a formally π-conjugated backbone, whereas a cross-conjugation framework is associated with the former type. The most intriguing difference between the two types of polymers relies in the fact that each donor group is directly conjugated to the pyridine nitrogen acceptor site in type I systems, whereas only one D group can delocalize its electron pair to the nitrogen atom in type II polymers.[13] Thus, three stable resonance structures can be written to describe the repeating unit in the former polymer as a consequence of the intramolecular charge transfer (ICT) from D to A, while only two structures are possible in the latter case. We therefore expect different properties for the two types of macromolecules. As a donor group we have relied on the favorable described properties of the EDOT ring. On this basis we have investigated the D−A−D type I polymer **P(2,6-Py-V-EDOT)** and type II polymer **P(2,5-Py-V-EDOT)** (Scheme 2).

Synthesis of Monomers and Polymers. The syntheses of the monomers **2,6-Py-V-EDOT** and **2,5-Py-V-EDOT** are shown in Scheme 2. **2,6-Py-V-EDOT** was obtained through a one-pot double Horner-Emmons condensation of tetraethyl 2,6-bis(methanephosphonate)pyridine (**1**)[22] with two equivalents of 3,4-ethylenedioxythiophene-2-carbaldeyde[23] using potassium *tert*-butoxide as a base. Similarly, a Horner-Emmons condensation between tetraethyl 2,5-bis(methanephosphonate)pyridine (**2**) and 3,4-ethylenedioxythiophene-2-carbaldeyde afforded in good yields the isomer **2,5-Py-V-EDOT**. In contrast to the 2,6-bis(phosphonate) pyridine derivative **1**, the analogous 2,5 derivative **2** was not previously reported in the literature. We readily obtained **2** in almost quantitative yields by refluxing 2,5-bis-(bromomethyl)pyridine[24] in neat triethylphosphite. The starting reagent 2,5-bis(hydroxymethyl)pyridine was prepared as previously described.[25]

The polymers **P(2,6-Py-V-EDOT)** and **P(2,5-Py-V-EDOT)** were synthesized by two different routes: oxidative electropolymerization and Yamamoto coupling (Scheme 2). The Yamamoto coupling polymerization was carried out on the corresponding dibromoderivatives **3** and **4**, obtained by bromination of the monomers with NBS in DMF, using bis(1,5-cyclooctadiene)-nickel(0) ($Ni(cod)_2$) as a catalyst.

Although our target was the use of as simple as possible constituting fragments (i.e., unsubstituted EDOT), in view of

Scheme 2. Synthesis of 2,6-Py-V-EDOT and 2,5-Py-V-EDOT and Corresponding Polymers P(2,6-Py-V-EDOT) and P(2,5-Py-V-EDOT)

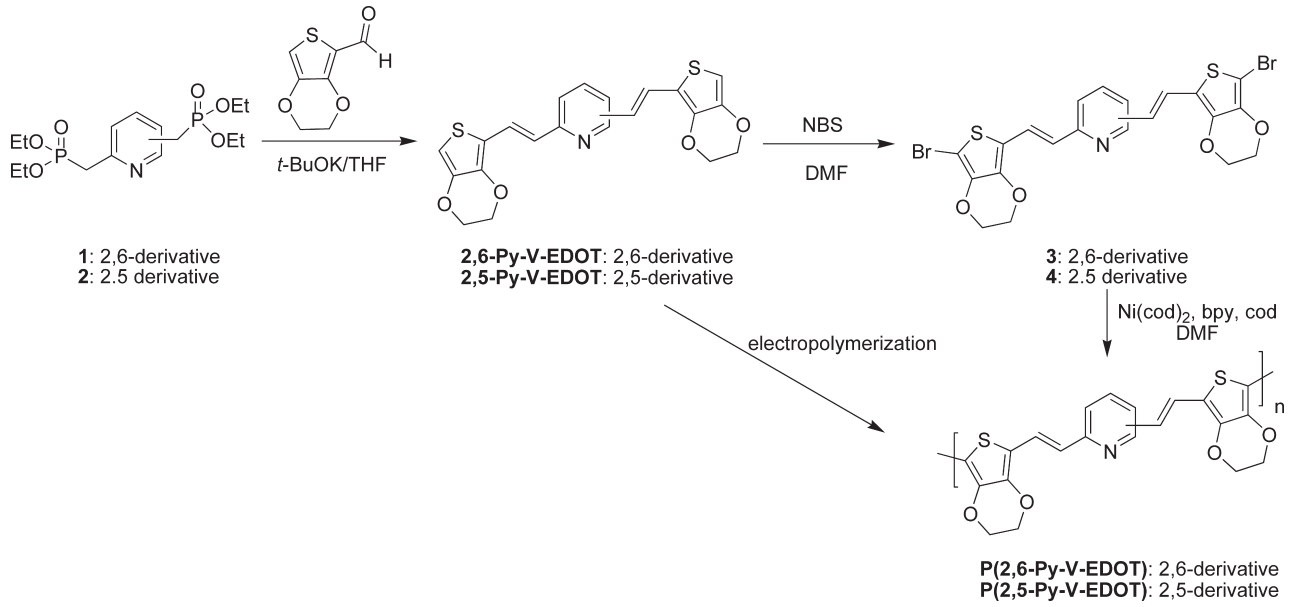

the investigation of the new polymers in BHJ photovoltaic cells we have also planned the synthesis of the corresponding more soluble monomer **2,6-Py-V-ProDOT**, where the EDOT group has been replaced by the dialkylated derivative of poly(3,4-propylenedioxythiophene) (ProDOT)[9a,b,10f,26] (Scheme 3). The ProDOT monomer was prepared similarly to their EDOT counterparts by Horner−Emmons condensation of tetraethyl bis(methanephosphonate)pyridine **1** and 3,4-(2,2-dihexylpropylenedioxy)thiophene-2-carbaldehyde.[9a] Unfortunately, our efforts to get the polymer **P(2,6-Py-V-ProDOT)** by oxidative electropolymerization or Yamamoto coupling failed. In fact, the low adhesion onto FTO coated glass substrates of the growing polymers, likely due to the presence of the two alkyl chains and to the high solubility in the electrolyte solution, prevented the formation of good quality films by electrochemical polymerization. With regard to the Yamamoto synthesis the bromination of **2,6-Py-V-ProDOT** under the same conditions as for the synthesis of **3** afforded a complex mixture of products, from which the desired precursor of the Yamamoto coupling could not be isolated. For these reasons and in order to compare homogeneous polymers as obtained by the two different routes (oxidative electropolymerization and Yamamoto coupling) we have decided to continue our investigation exclusively on the EDOT derivatives, despite their lower solubility in organic solvents.

NMR Spectroscopy of Monomers. The ^{1}H NMR spectra in different solvents and temperatures of the monomers **2,6-Py-V-EDOT** and **2,5-Py-V-EDOT** are shown in Figures 1 and 2, respectively. Traces of some minor byproduct, that could be likely identified as the *Z*,*Z* isomer (coupling constant J = 12.8 Hz for the vinyl protons) and the monocondensation product (as derived from anisochronous pyridine β protons), were recorded in the ^{1}H NMR spectrum of **2,6-Py-V-EDOT** in DMSO. Unfortunately, these minor impurities could not be completely removed by recrystallization or flash chromatography. As expected the spectra of the two isomeric monomers have a different number of signals depending on the molecular symmetry. More importantly, the two spectra diverge depending on the nature (type-I vs type-II; see Scheme 1) of the monomer. Indeed, in **2,6-Py-V-EDOT** the two zwitterionic resonance structures ZW−A and ZW−B (Scheme 4) are equivalent; both EDOT rings are involved, to the same extent, in the ICT to the acceptor

Scheme 3

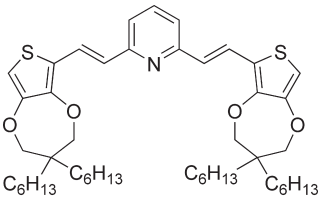

2,6-Py-V-ProDOT

pyridine nitrogen atom. In **2,5-Py-V-EDOT** the picture is rather different since now the oxygen lone pair of only one EDOT ring can be directly delocalized to the pyridine nitrogen atom, and therefore only one stable zwitterionic limit formula (ZW) can be written (Scheme 4). It is therefore expected that the bond between C(2) of the EDOT ring and the adjacent ethenylic spacer should have a higher double-bond character for the directly conjugated donor heterocycle (ring A in Scheme 4) than for the second nonconjugated EDOT ring (ring B). In turn, this leads to hindered rotation around the former bond and to the possible presence of two geometric isomers with different chemical shifts.

The NMR analysis elegantly confirms the whole picture. The ^{1}H NMR spectrum of **2,6-Py-V-EDOT** (Figure 1) does not show any important broadening of the signals and hence no hindered rotation. In contrast, one of the two EDOT−vinylene moieties in **2,5-Py-V-EDOT** clearly shows broadening of the proton signals, evidence of hindered rotation between EDOT C(2) and the vinylene unit. The broad signals are clearly assigned to the acceptor-conjugated EDOT ring A according to previous discussion. The broadening effect is more evident as the polarity of the solvent increases ($CH_2Cl_2 \rightarrow$ DMSO), as a consequence of the higher contribution of the zwitterionic form and thus of the larger rotational barrier along the EDOT C(2)-vinylene bond. Variable-temperature dependent experiments in DMSO have confirmed the presence of the rotameric equilibria in **2,5-Py-V-EDOT**.

Optical and Electrochemical Characterization of Monomers. The monomers **2,6-Py-V-EDOT** and **2,5-Py-V-EDOT** show a strong ICT absorption band in the Vis spectral region and no near-IR absorption. They both present a fluorescence

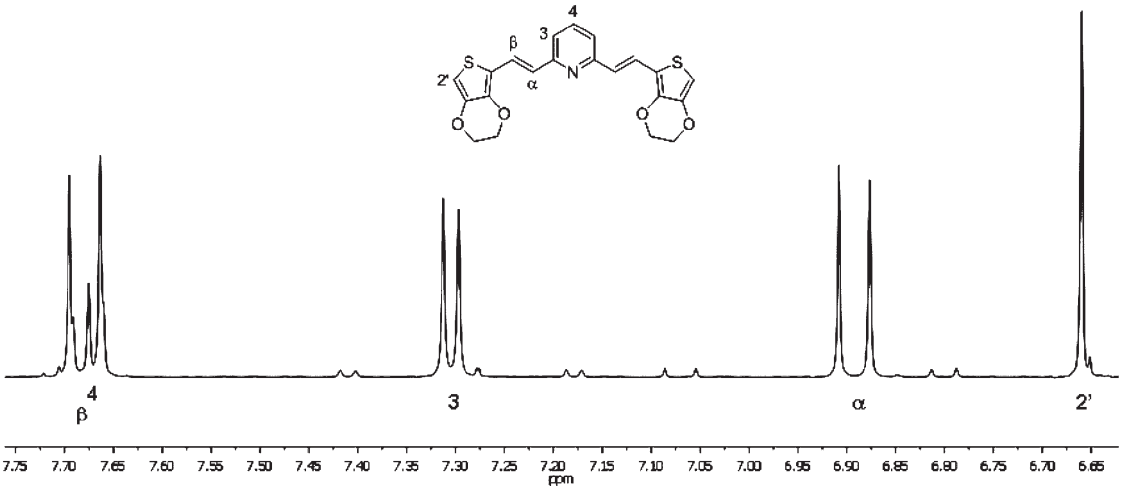

Figure 1. ^{1}H NMR spectrum of monomer **2,6-Py-V-EDOT** in DMSO at 25 °C (aromatic region).

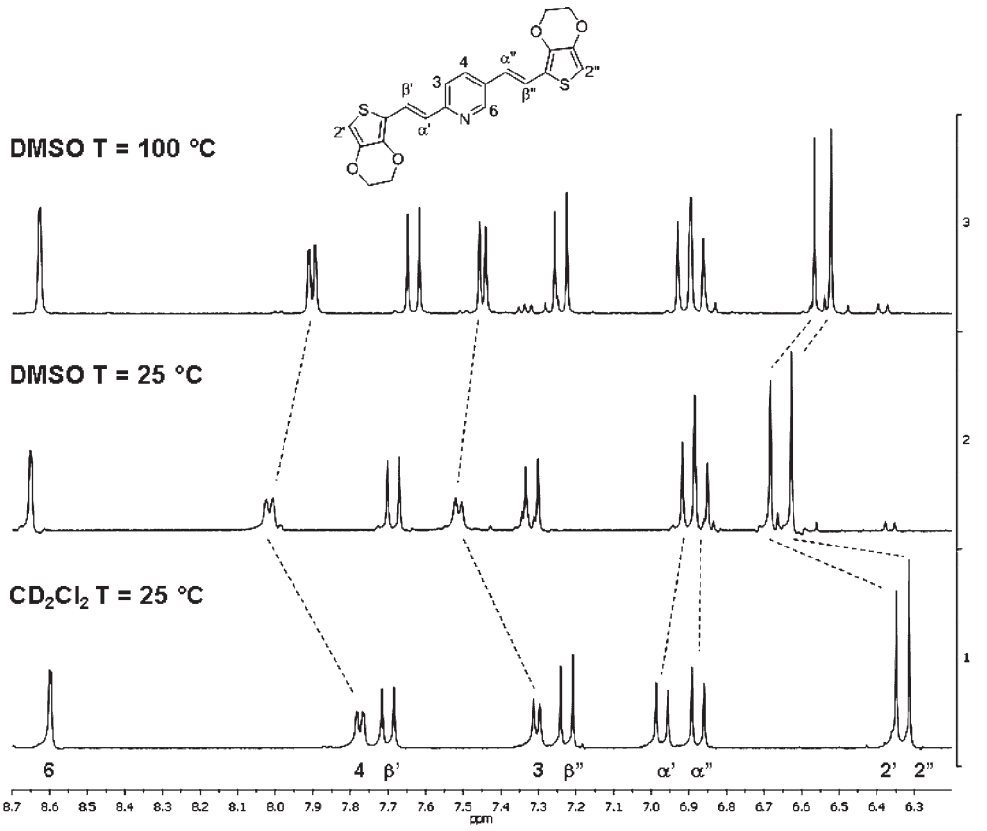

Figure 2. ^{1}H NMR spectra of monomer **2,5-Py-V-EDOT** in $CDCl_2$ (25 °C) and DMSO (25 and 100 °C) (aromatic region).

emission, with modest fluorescence quantum yields. Table 1 lists the main optical data of the two monomers in solution. The absorption and emission spectra of the two monomers are shown in Figure 3. Spectra were also recorded upon addition of a large excess of Et_3N to check against pyridine protonation.

As can be seen from the optical data, the 2,5-substitution pattern around the central pyridine core, corresponding to a *para* relative position of the two EDOT−vinylene donor substituents, induces a bathochromic shift by 69 nm and a hyperchromic effect with respect to the 2,6-derivative (*meta* substitution). Such bathochromic effect decreases the estimated optical bandgap and 0−0 transition energy by 0.2 eV on going from **2,6-Py-V-EDOT** to **2,5-Py-V-EDOT**.

Cyclic Voltammetry (CV) was performed on monomer solutions to determine polymerization potentials and currents (see also Supporting Information). Both **2,6-Py-V-EDOT** and **2,5-Py-V-EDOT** show, during the first oxidative scan, a two-step oxidative process with the first peak at 0.80 and 0.55 V, respectively. During the first cathodic scan a small negative current is recorded, which was ascribed to the reduction of the freshly formed polymer layer onto the FTO surface. From the second scan the curves are more complicated due to the overlap of the polymer and the monomer (or oligomer) oxidative processes. The HOMO values for the monomers (Table 1) were obtained from the CV first oxidative branch (onset of the oxidation processes). The LUMO energies were estimated by the HOMO values by adding the 0−0 transition energies.

Scheme 4. Neutral and Zwitterionic Resonsance Structures of 2,6-Py-V-EDOT and 2,5-Py-V-EDOT

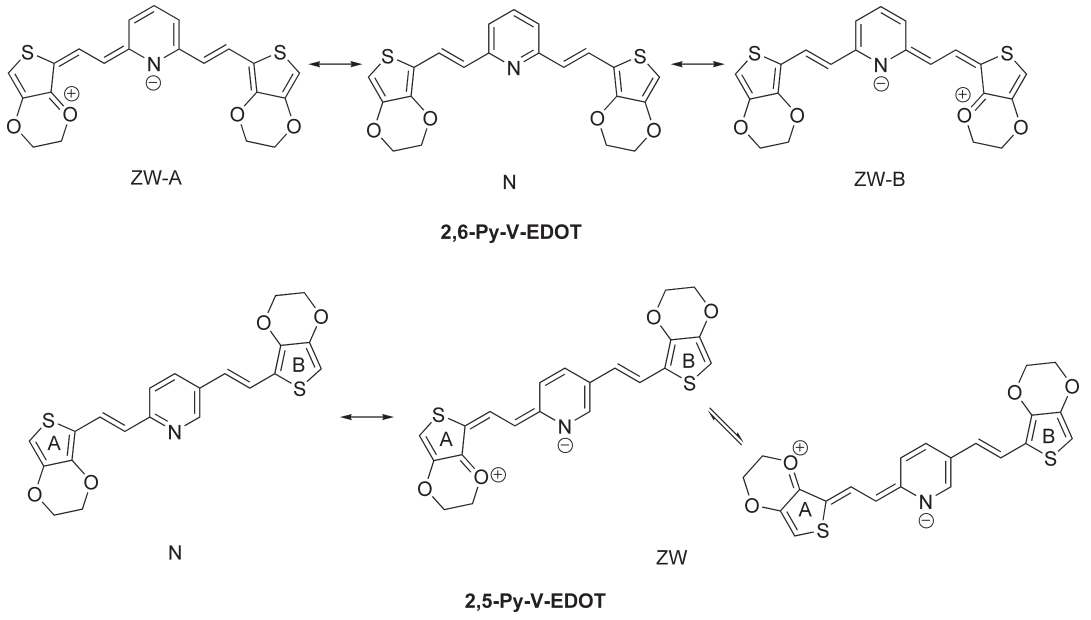

Table 1. Optical ($CHCl_3$) and Electrochemical (CH_3CN) Properties of the Monomers 2,6-Py-V-EDOT and 2,5-Py-V-EDOT

compd	λ_{max}(abs)[a] [nm]	λ_{onset} (abs) [nm]	E_{gap}^{opt} [b] [eV]	λ_{max}(em)[c] [nm]	$E_{(0-0)}$ [d] [eV]	E_{onset}^{ox} [e] [V]	HOMO[f] [eV]	LUMO[g] [eV]
2,6-Py-V-EDOT	334 (31 200)	425	2.9	434 (0.07)	3.0	0.60	−5.8	−2.8
2,5-Py-V-EDOT	403 (41 500)	460	2.7	486 (0.11)	2.8	0.40	−5.6	−2.8

[a] Extinction coefficient ε [mol^{-1} L cm^{-1}] in parentheses. [b] Optical bandgap (calculated on the low energetic edge of the absorption spectrum). [c] Fluorescence quantum yield Φ in parentheses (DMSO); coumarin 540A was used as a standard (Φ = 0.58 in EtOH). [d] 0−0 Transition energy estimated from the intercept of the normalized absorption and emission spectra. [e] Vs. Fc/Fc^+. [f] HOMO energies are derived from the electrochemical data based on the assumption that the Fc/Fc^+ redox couple is 5.2 eV relative to vacuum. [g] Estimated from HOMO and 0−0 transition energy.

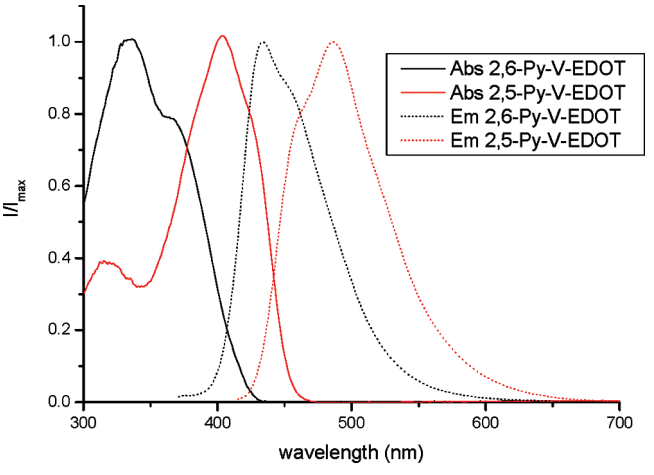

Figure 3. Normalized absorption and emission spectra of **2,6-Py-V-EDOT** and **2,5-Py-V-EDOT** in $CHCl_3$.

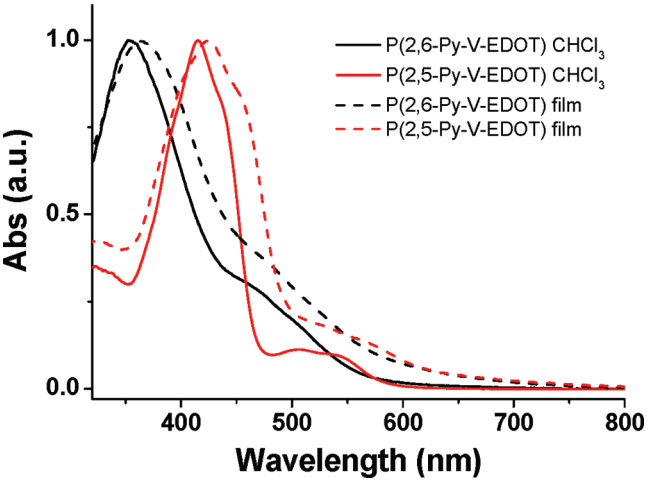

Figure 4. Absorption spectra of **P(2,6-Py-V-EDOT)** and **P(2,5-Py-V-EDOT)** measured in $CHCl_3$ solution (solid line) and as thin film (dashed line).

In conclusion, NMR, optical, and electrochemical data converge in demonstrating the structural and electronic different behavior of the two monomers induced by the different substitution pattern on the central electron-acceptor moiety, hence predicting different properties of the corresponding polymers, in agreement with one of the main scopes of this work. Ab-initio computations confirm the described experimental behavior (vide infra).

Chemical Characterization and Optical Properties of Polymers. The polymers obtained via Yamamoto coupling were submitted to ^1H NMR spectroscopy (Supporting Information), UV−vis spectroscopy, GPC, DSC, and TGA characterization (see Experimental Section). UV−vis spectra of polymers measured both in $CHCl_3$ solution and as thin films are shown in Figure 4. Absorption spectra were also recorded, with no deviation, in the presence of a base (Et_3N) to rule out protonation of the pyridine nitrogen. Optical data, molecular weights, thermal transitions, and thermal stability data of chemically obtained **P(2,6-Py-V-EDOT)** and **P(2,5-Py-V-EDOT)** are collected in Table 2.

The GPC data revealed that the isolated species ($CHCl_3$ fraction) obtained via Yamamoto coupling have rather low molecular-weights. This is due to the presence of unsubstituted

Table 2. Structural and Optical Properties of P(2,6-Py-V-EDOT) and P(2,5-Py-V-EDOT), Obtained Via Yamamoto Polymerization, in $CHCl_3$ Solution and as Thin Film

					$CHCl_3$ solution			film				
	M_w[a] [kg mol^{-1}]	M_n[b] [kg mol^{-1}]	PDI[c]	av no. of repeat units	λ_{max} [nm]	λ_{onset} [nm]	E_{gap}^{opt}[d] [eV]	λ_{max} [nm]	λ_{onset} [nm]	E_{gap}^{opt}[d] [eV]	T_g[e] [°C]	T_d[f] [°C]
P(2,6-Py-V-EDOT)	5.21	5.04	1.03	12	353	650	1.9	364	760	1.6	110	240
P(2,5-Py-V-EDOT)	2.33	2.27	1.03	6	415	615	2.0	424	770	1.6		265

[a] Weight-average molecular weight obtained by GPC. [b] Number-average molar mass obtained by GPC. [c] Polydispersity index (PDI = M_w/M_n). [d] Optical bandgap (calculated on the low energetic edge of the absorption spectrum). [e] Glass transition temperature determined by DSC. [f] Decomposition temperature determined by TGA (5% weight loss).

Table 3. Electrochemical Properties of Electrochemically Polymerized P(2,6-Py-V-EDOT) and P(2,5-Py-V-EDOT), in 0.1 M (TBA)PF_6 CH_3CN Solution[a]

polymer	E_{onset}^{ox} [V]	HOMO [eV]	E_{onset}^{red} [V]	LUMO [eV]	E_{gap}^{EC}[b] [eV]
P(2,6-Py-V-EDOT)	−0.23	−5.0	−1.80	−3.4	1.6
P(2,5-Py-V-EDOT)	−0.11	−5.1	−1.78	−3.4	1.7

[a] All potentials are reported vs Fc/Fc^+ and HOMO and LUMO energies are derived from the electrochemical data based on the assumption that the Fc/Fc^+ redox couple is 5.2 eV relative to vacuum. [b] Electrochemical bandgap, obtained from the difference between the reduction and the oxidation potential onset (or LUMO and HOMO energies).

EDOT rings which led to polymers with limited solubility. In particular, only the fraction of **P(2,5-Py-V-EDOT)** corresponding to ~6 repeat units could be isolated. In fact, relatively large quantities of solid remained in the Soxhlet extraction thimble after chloroform extraction. This solid, although endowed with significantly red-shifted absorption spectrum, thus suggesting the presence of higher molecular weight species, was not soluble in any solvent and could not be used for the subsequent investigation. **P(2,6-Py-V-EDOT)** was alternatively prepared by Horner−Emmons polycondensation of tetraethyl 2,6-bis(methanephosphonate)pyridine (**1**)[22] with 2,2′-bis(3,4-ethylenedioxy)thienyl-5,5′-bis(carbaldehyde)[27] but even lower molecular weight species could be isolated. As previously described, our efforts for preparing more soluble derivatives were not successful (vide infra).

The ^1H NMR spectra of the polymers (Supporting Information) are in good agreement with the GPC molecular weight data. In fact, broad bands have been recorded for the higher molecular weight polymer **P(2,6-Py-V-EDOT)**. In contrast, rather sharp signals with full assignment (Figure S18, Supporting Information) were obtained for the 2,5-derivative, in agreement with a hexamer structure. The low average number of repeat units likely explains the small bathochromic shift (12 - 19 nm) of the absorption peak ($CHCl_3$ solution) of the Yamamoto polymers with respect to the corresponding monomers, although their optical bandgaps significantly decrease from 2.9 and 2.7 eV (Table 1) to 1.9 and 2.0 eV (Table 2) in **P(2,6-Py-V-EDOT)** and **P(2,5-Py-V-EDOT)**, respectively. We must then conclude that the Yamamoto polymers, when investigated in solution, could not be considered low bandgap polymers, being their optical gaps equal or close to the value of 2.0 eV. However, when measured as thin films, absorption peaks are further red-shifted by ~10 nm and optical bandgaps are lowered to 1.6 eV, in excellent agreement with the electrochemical bandgaps obtained on the electrochemically polymerized species (1.6 and 1.7 eV) (Table 3), as described in the following section. Thermogravimetric analysis (TGA) and differential scanning calorimetry (DSC) were performed to evaluate the thermal stability and thermal transitions of the Yamamoto products. **P(2,6-Py-V-EDOT)** and **P(2,5-Py-V-EDOT)** exhibit satisfying stability with an onset decomposition temperature (5% weight loss) at 240 and 265 °C, respectively. This level of thermal stability is adequate for applications in OPVs and other optoelectronic devices. **P(2,6-Py-V-EDOT)** shows a glass transition temperature (T_g) of 110 °C, whereas no glass transition-like feature was observed in the DSC scans of **P(2,5-Py-V-EDOT)**, again in agreement with its oligomeric nature.

Electrochemical Characterization of Polymers. Thin films of **P(2,6-Py-V-EDOT)** and **P(2,5-Py-V-EDOT)** were obtained by electrochemical polymerization onto FTO coated glass substrates starting from solutions of the corresponding monomers. The new polymers were characterized by CV in a monomer-free electrolyte solution by varying the potential scanning in the p-doping zone between +0.28 and −0.86 V and in the n-doping zone between −0.76 and −2.05 V. The potential ranges were carefully selected in order to maximize the layer stability by measuring the charge flow in both anodic and cathodic CV branches. CV curves of **P(2,6-Py-V-EDOT)** and **P(2,5-Py-V-EDOT)**, prepared under galvanostatic conditions at 0.1 mA cm^{-2} and 7 mC cm^{-2}, are shown in Figure 5 both for the p- and n-doping potential region (fifth scan) in monomer-free electrolyte solutions. Further CV cycles did not show any significant current change.

Both polymers exhibit a reversible p-doping/dedoping process with onset potentials at −0.1/−0.2 V vs Fc/Fc^+. Sharp charge trapping like-peaks have been recorded in CV of **P(2,5-Py-V-EDOT)** as well.[10a] In contrast, the n-doping behavior, taking place at onset potential of ca. −1.8 V vs Fc/Fc^+, was different depending on the type (I vs II) of the polymer. The optical characterization of the monomers has pointed out that the 2,5-pyridine (*para* substitution) core allows for better conjugation between the donor EDOT fragments with respect to the 2,6-pyridine core. As a consequence of the more efficient π-conjugation pattern, the reduction of **P(2,5-Py-V-EDOT)** was partially reversible, whereas no anodic current was observed for **P(2,6-Py-V-EDOT)** (Figure 5b). In summary, the type II monomer **2,5-Py-V-EDOT** is able to yield polymers with higher conjugated n-doped states, the doping process of which is more reversible.

The electrochemical properties (onset of oxidation and reduction potential) and derived HOMO, LUMO and bandgap energies of **P(2,6-Py-V-EDOT)** and **P(2,5-Py-V-EDOT)** are collected in Table 3. HOMO/LUMO energies in comparison with those of PCBM are pictorially summarized in Figure 6. Despite the fact the two monomers—and corresponding polymers—show somewhat different optical and electrochemical (see n-doping behavior) properties, the oxidation and reduction potential onsets and, accordingly, derived HOMO and LUMO energies, are very similar to each other. As expected, polymerization raises the HOMO

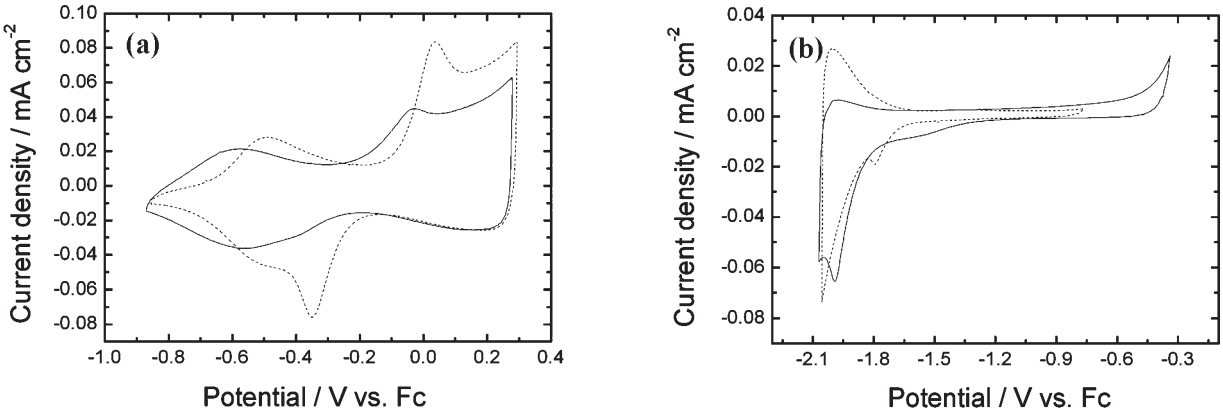

Figure 5. Cyclic voltammetries in 0.1 M monomer-free electrolyte solution at 50 mV s^{-1} of **P(2,6-Py-V-EDOT)** (solid line) and **P(2,5-Py-V-EDOT)** (dashed line): (a) positive potential (p-doping) scan; (b) negative potential (n-doping) scan.

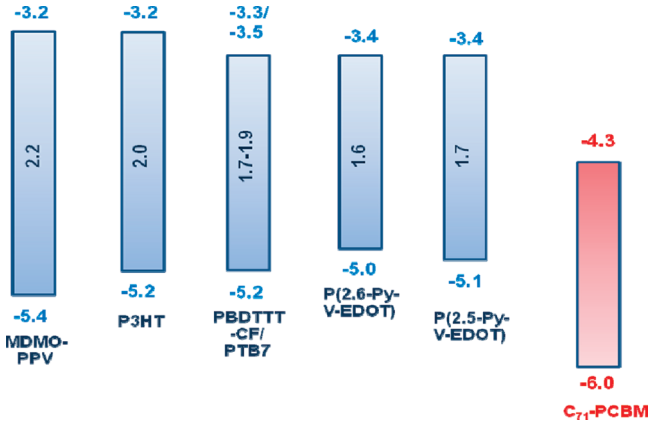

Figure 6. HOMO, LUMO, and bandgap energies (eV) of **P(2,6-Py-V-EDOT)** and **P(2,5-Py-V-EDOT)** in comparison with reference polymers as the donors and PCBM as the acceptor.

and lowers the LUMO energies with respect to the monomers (Table 1). The LUMO energies are identical in the two polymers and both higher than that of PCBM by more than 0.3 eV (minimal offset), fitting one of the main requirements for use in OPVs.

The recorded HOMO and LUMO values can be compared with those of the most commonly used donor polymers in BHJ photovoltaic cells: poly[2-methoxy-5-(3,7-dimethyloctyloxy)-*para*-phenylene]vinylene) (MDMO−PPV) and poly(3-hexylthiophene) (P3HT).[2] The HOMO, LUMO, and bandgap energies of MDMO−PPV and P3HT are included in Figure 6. It can be easily seen that the HOMO energy is higher in **P(2,6-Py-V-EDOT)** and **P(2,5-Py-V-EDOT)** than in P3HT (and MDMO−PPV), due to the stronger electron-rich nature of EDOT with respect to the alkylthiophene ring in P3HT. At the same time the presence of the acceptor pyridine group lowers the LUMO energies with respect to the all-donor MDMO−PPV and P3HT polymers. The net result is a decrease of the bandgap energy by up to 0.6 eV. We can therefore conclude that the new polymers fit very well the energy levels requirements for enhanced performances in BHJ solar cells using PCBM as acceptor, namely LUMO energies sufficiently higher than $LUMO_{PCBM}$ and bandgaps equal or lower than 1.7 eV. Interestingly, the estimated molecular orbitals and bandgap energies of both **P(2,6-Py-V-EDOT)** and **P(2,5-Py-V-EDOT)** are very similar to those of donor copolymer PBDTTT−CF[20] or PTB7,[21] which holds the current record efficiency in polymer solar cells.

Spectroelectrochemistry was performed on the stable polymers **P(2,6-Py-V-EDOT)** and **P(2,5-Py-V-EDOT)** at various applied potentials (Figure 7). The recorded spectra are similar for both polymers, with three main absorption peaks present in the visible region at ca. 350, 530, and 730 nm. When oxidative potentials are applied, an increase of the absorption peak at 730 nm was observed. Typically, absorption in this region is due to localized polaronic states formed by partial oxidation of the neutral polymers.[12] However, the formation of the bipolaronic low energy band was not recorded even at the highest applied oxidation potentials. This can be due to uncomplete oxidation of the polymeric chains and breaking of the conjugated donor−donor path due to the presence of the acceptor groups along the backbone. In other terms, the polymers are prone to store less positive charge with respect to full donor conducting polymers.

DFT/TDDFT Calculations. To gain insight into the structural, electronic, and optical properties of the investigated systems, we performed DFT/TDDFT calculations, including solvation effects, on the monomers **2,6-Py-V-EDOT** and **2,5-Py-V-EDOT** and their selected oligomers **(2,6-Py-V-EDOT)$_n$** and **(2,5-Py-V-EDOT)$_n$**, with the aim to simulate experimental properties of the polymeric species. The theoretical study of a polymeric system can be performed via two different approaches: (i) by considering the infinite polymer as a periodic system, and (ii) by analyzing extended systems with increasing but finite dimension. Here, we chose the second approach, where the polymer is studied with a growing up approach starting from the principal monomeric unit. This "cluster" approach[28] allows us to exploit all the computational machinery developed for isolated systems, including the calculation of excited states using the time-dependent DFT and to include solvation effects in a simple yet effective way, by means of the polarizable continuum model (PCM).[29]

Geometry optimization in vacuo of the monomers was performed by the B3LYP functional using both 3-21G* and 6-31G* basis sets, finding minimal differences between the two data sets. The use of reduced basis sets is very important for the description of the extended oligomeric systems, whereby a large number of atoms need to be considered and thus a large associated computational overhead. The optimized geometries of representative systems are shown in Figure 8. The optimized structures are planar in all cases, apart from the EDOT groups which have a tridimensional geometry.

On the optimized geometries of the monomers and oligomers, composed by up to six monomeric units (n = 6), we performed TDDFT excited state calculations (Table 4). For

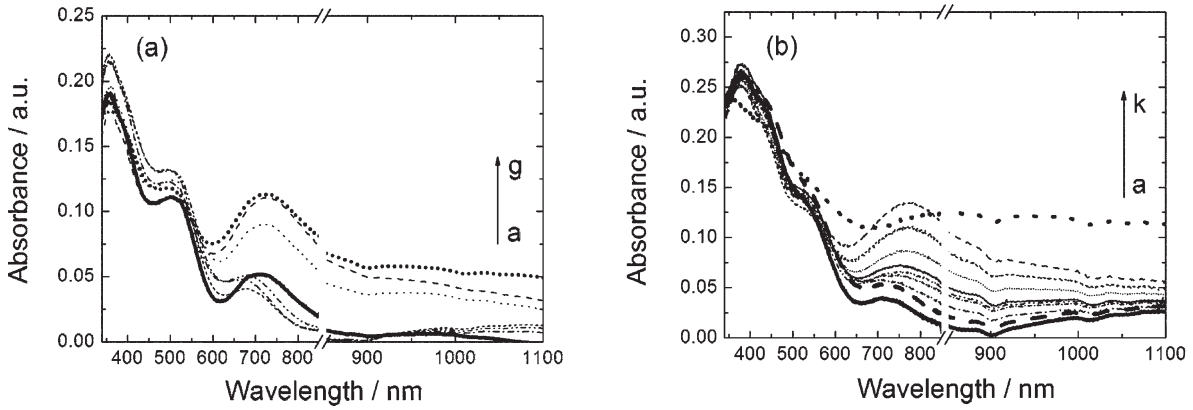

Figure 7. Spectroelectrochemistry of (a) **P(2,6-Py-V-EDOT)** and (b) **P(2,5-Py-V-EDOT)** on FTO in monomer-free 0.1 M $(TBA)PF_6/CH_3CN$ electrolyte at consecutive applied potentials. Left, a: (a) open circuit potential, (b) +0.6, (c) +0.2, (d) −0.5, (e) −1.7, (f) −0.5, and (g) 0.6 V vs Fc/Fc^+. Right, b: (a) open circuit potential, (b) +0.5, (c) +0.2, (d) −0.5, (e) +0.2, (f) +0.5, (g) 0, (h) −0.5, (i) −1.0, (j) −1.5, and (k) −2.0 V vs Fc/Fc^+. The break along the wavelength axis between 800 and 900 nm is due to the change between visible and IR detectors.

the **2,6-Py-V-EDOT** and **2,5-Py-V-EDOT** monomers, absorption maxima are measured at 3.71 and 3.08 eV, respectively. By using the B3LYP functional, we calculated lowest excitation energies in vacuo (solution) of 2.95 (2.80) eV and 2.91 (2.79) eV, respectively. This discrepancy was traced back in our previous work[30] to an incorrect description of the excited states with a strong delocalization of π electrons. In the same work, we found that B3LYP provides accurate ground state geometries, whereas the MPW1K functional, which has an increased percentage of Hartree−Fock exchange, provides excitation energies in much closer agreement with experimental values.[30a] Therefore, we repeated TDDFT calculations for **2,6-Py-V-EDOT** and **2,5-Py-V-EDOT** finding lowest excitation energies (Table 4), in excellent agreement with the experimental values.

Concerning the electrochemical properties, there are two ways to estimate the oxidation/reduction potentials: (i) the vertical approximation due to the Koopmans theorem, i.e., by taking the negative of the HOMO and LUMO single particle eigenvalues, and (ii) by moving forward to the simple single orbital energies and calculating the real oxidation and reduction Gibbs free energy differences, which are the quantities effectively corresponding to the measured adiabatic oxidation and reduction potentials, involving geometrical relaxation of the oxidized and reduced species. Both approaches have their merits, with Koopmans theorem offering a simple but approximate computational procedure, requiring only a calculation on the neutral species. The calculation of Gibbs free energies, on the other hand, is accurate but computationally very intensive, requiring calculation of geometries and vibrational frequencies in vacuo and geometries in solution, for both the neutral, cation, and anion species. We have tested both approaches for the monomers and trimers, the latter being the largest systems for which calculation of Gibbs free energies is possible within a reasonable computer overhead.

The computed B3LYP/6-31G* HOMO and LUMO levels of **2,6-Py-V-EDOT** and **2,5-Py-V-EDOT** are listed in Table 4 (n = 1) (see Figure 10 for isodensity contour plots). For **2,5-Py-V-EDOT**, calculation of the oxidation potentials at the B3LYP/6-311++G** level leads to a value of 5.26 eV (to be compared to a corresponding HOMO value of −5.33 eV). For the **2,6-Py-V-EDOT** monomer, we have not been able to calculate the corresponding Gibbs free energy of oxidation, due to technical problems with the solvation model. We notice that the calculated single particle HOMO values are in reasonable agreement with the experimental estimates (Table 1). Most notably we are able to reproduce the ca. 0.2 eV HOMO stabilization occurring in **2,6-Py-V-EDOT** compared to **2,5-Py-V-EDOT**. It is worthy noting that for **2,5-Py-V-EDOT** the calculation of the Gibbs free energy difference leads to an estimate of the oxidation potential of −5.15 eV, in slightly better agreement with the experimental value than the single particle approximation. Overall, both approaches seem to be adequate to describe the investigated systems, especially considering the somewhat uncertain conversion between relative measured electrochemical potentials and absolute values referred to the vacuo. A comparison between calculated LUMOs and the corresponding experimental estimates is not possible for the monomers, since the experimental data are a combination of electrochemical and optical data.

Having established the relative accuracy of our computational set up, we then adopted the selected hybrid level of theory to extended our investigations to the whole oligomer series, from the dimer (n = 2) to the hexamer (n = 6) (Table 4). We computed a strong reduction of the excitation energy moving from the monomer to the dimer (ca. 1 eV) and a smaller decrease from the dimer to the hexamer. As reported in the literature,[31] using a linear fit and plotting the excitation energy against 1/n we can extrapolate the values of the infinite polymer as the intercept with ordinate axes (Figure 9). The calculated extrapolated values of the absorption energies in solution (Table 4, fit n = 1−5) are consistent with the experimental absorption onsets, located at ca. 2 eV for both systems, although it is quite difficult to compare these values due to the different absorption shapes experimentally recorded for the two systems.

Concerning the oxidation potentials, we notice that a rather drastic reduction of such quantities is observed on going from the monomer to the oligomeric species, with differences of ca. −0.8 eV, in agreement with the trend of measured quantities. Considering extrapolated HOMOs values, we retrieved the same 0.2 eV difference in oxidation potential between **P(2,6-Py-V-EDOT)** and **P(2,5-Py-V-EDOT)** as found for the monomers. Calculation of the oxidation Gibbs free energy differences for n = 3 leads to values of 4.71 and 4.57 eV for **P(2,6-Py-V-EDOT)** and **P(2,5-Py-V-EDOT)**, respectively, with a trend analogous to that observed for the monomers. Similarly, LUMO energies are computed to decrease by up to 0.5−0.6 eV as the number of units increase. The extrapolated LUMO values in THF (Table 4) can be compared to the calculated (n = 3) reduction Gibbs free energy difference of 2.59 and 2.46 eV for **P(2,6-Py-V-EDOT)** and **P(2,5-Py-V-EDOT)**, respectively.

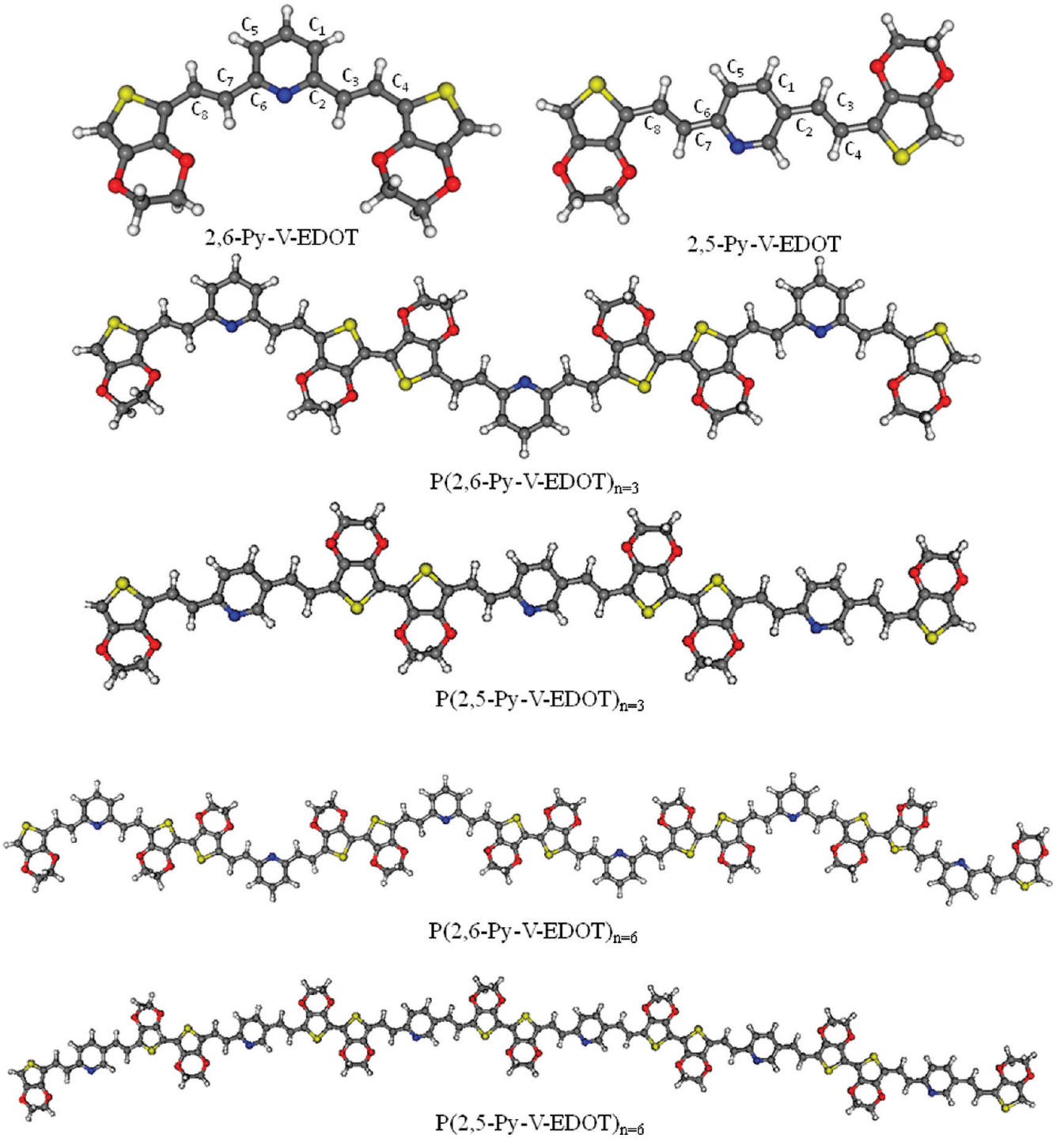

Figure 8. Optimized geometries of **2,6-Py-V-EDOT** and **2,5-Py-V-EDOT** monomers and oligomers.

By combining the calculated information and comparing with experimental data we conclude that the calculated oxidation/reduction potentials are too positive, even though a nice correlation between calculated and experimental data can be obtained, especially for **P(2,5-Py-V-EDOT)**, for which an almost rigid upshift of calculated quantities of ca. 0.9 eV is calculated (remember however the conversion between electrochemical potentials and absolute energy values), providing essentially the same HOMO−LUMO gap as experimentally found. The situation is definitely less clear for **P(2,6-Py-V-EDOT)**, for which the computed HOMO and LUMO energies are higher by 0.6 and 1.2 eV, respectively, leading to a predicted HOMO−LUMO gap of 2.2 eV compared to the experimental value of 1.6 eV. This difference is not related to the ground state geometries, since the same behavior has been retrieved considering Hartree−Fock and, for the monomers and dimers, MP2 optimized geometries (Supporting Information), and might be due to an intrinsic limitation of DFT in describing charge-delocalization in the specific case of **P(2,5-Py-V-EDOT)**.

Photovoltaic Properties. The potential of semiconductors **P(2,5-Py-V-EDOT)** and **P(2,6-Py-V-EDOT)** as donor materials in OPV devices was investigated in BHJ solar cells using C_{71}−PCBM as the acceptor. The devices were fabricated with the standard configuration of glass/ITO/PEDOT:PSS/DONOR:PCBM/LiF/Al. The active layer films were spin-coated from chloroform solutions in ambient conditions (chloroform

Table 4. Calculated HOMO,[a] LUMO,[a] and Excitation Energies[b] of (2,6-Py-V-EDOT)$_n$ and (2,5-Py-V-EDOT)$_n$

	(2,6-Py-V-EDOT)$_n$				(2,5-Py-V-EDOT)$_n$			
n	excitation energy [eV]	HOMO [eV]	LUMO [eV]	E_{gap} [eV]	excitation energy [eV]	HOMO [eV]	LUMO [eV]	E_{gap} [eV]
1	3.67	−5.17	−1.65	3.52	3.11	−4.97	−1.92	3.06
	(3.79)	(−5.00)	(−1.47)	(3.53)	(3.23)	(−4.81)	(−1.74)	(3.07)
2	2.69	−4.68	−2.03	2.65	2.40	−4.55	−2.21	2.34
	(2.79)	(−4.57)	(−1.81)	(2.66)	(2.48)	(−4.36)	(−2.02)	(2.35)
3	2.61	−4.63	−2.05	2.58	2.22	−4.44	−2.30	2.14
	(2.67)	(−4.42)	(−1.83)	(2.59)	(2.28)	(4.25)	(−2.10)	(2.15)
4	2.57	−4.61	−2.06	2.55	2.15	−4.4	−2.34	2.06
	(2.62)	(−4.40)	(−1.84)	(2.56)	(2.20)	(−4.20)	(−2.13)	(2.07)
5	2.55	−4.60	−2.07	2.54	2.11	−4.37	−2.36	2.02
	(2.59)	(−4.38)	(−1.84)	(2.55)	(2.15)	(−4.17)	(−2.14)	(2.03)
6								
		(−4.38)	(−1.84)	(2.55)		(−4.20)	(−2.18)	(2.02)
fit n = 1−5	2.16	−4.41	−2.21	2.20	1.82	−4.20	−2.48	1.72
	(2.19)	(−4.17)	(−1.97)	(2.20)	(1.84)	(−3.99)	(−2.26)	(1.73)
fit n = 1−6								
		(−4.20)	(−1.95)	(2.25)		(−4.01)	(−2.26)	(−1.74)

[a] HOMO and LUMO energies in THF (in vacuo in parentheses) calculated at the B3LYP/6-31G level on the B3LYP/3-21G* optimized geometries. [b] TDDFT excitation energies calculated at the B3LYP/3-21G* level with the MPW1K functional.

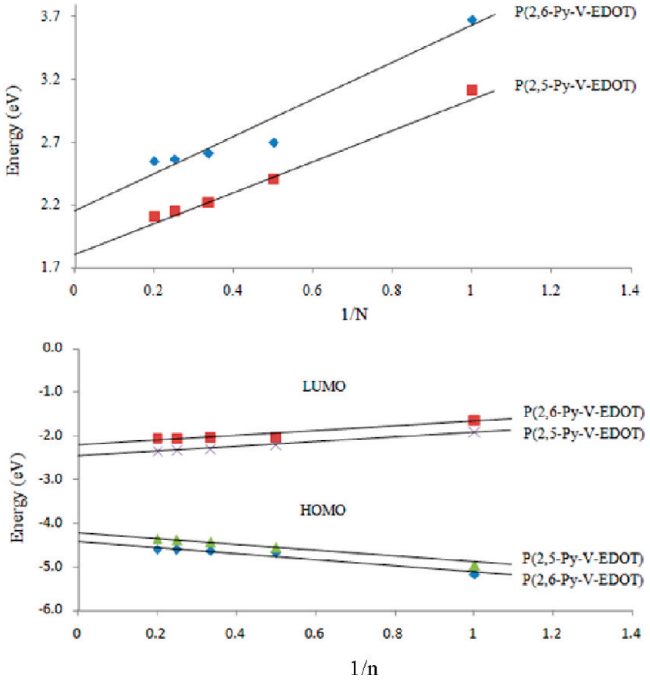

Figure 9. Calculated trends of HOMOs and LUMOs values (bottom) and of lowest excitation energies (top).

was found to be the optimum solvent). Device fabrication details are given in the Experimental Section. Figure 11 shows the current density−voltage plots for the optimized devices measured under AM 1.5G illumination. The corresponding photovoltaic parameters and PCEs are summarized in Table 5.

The performance is clearly dependent both on the donor material and on the blend composition. For both polymers, the highest efficiencies were achieved for devices based on 1:4 blend w/w ratio and without additional thermal treatments. Further increasing the PCBM content in the polymer blends led to a significant decrease of the short circuit current densities, thus resulting in lower PCEs. The blended films exhibited substantial poor FF values which were probably due to the low molecular weights of the polymers, thus resulting in film-forming qualities with limited nanoscale morphology, phase separation, and thereby electrical properties.[10o] Several efforts to optimize the thin-film morphology were carried out but without significant improvements. Active layer thermal annealing over the range 50−100 °C, and for different times, invariably resulted in extensive film degradation, adversely affecting J_{sc}, FF, and consequently the overall device performance. Moreover, higher-boiling point solvents (e.g., toluene, chlorobenzene, and *o*-dichlorobenzene) were used to spin-cast the blends but poor quality films were obtained as a consequence of the lower solubility of the polymers in these solvents. The most continuous and most electrically uniform films were here obtained from chloroform solutions, resulting in the best OPV performance. In order to evaluate, and eventually prevent, the possible detrimental chemical interactions between PEDOT:PSS (acidic properties) and the pyridine rings (basic sites) of the donors, that can influence the hole extraction efficiency, we investigated the performances of devices fabricated using MoO_3 as an alternative anode interfacial layer. Several groups have demonstrated that metal oxides (*e.g.*, NiO_x, MoO_3, and V_2O_5) can be efficiently used in OPVs to replace PEDOT:PSS as an anode interfacial layer.[32] Here, we investigated the performance of vapor deposited MoO_3 (∼5, 10, or 15 nm) as a buffer layer in devices made with the best **P(2,5-Py-V-EDOT)**:C_{71}−PCBM blend ratio (1:4 wt/wt) (see Figure S23 and Table S12 in the Supporting Information). In this device architecture, the most efficient solar cells (∼5 nm MoO_3) exhibited V_{oc} (0.55 V) and FF (35%) values nearly identical to those obtained for the PEDOT:PSS-based devices (Table 5), while the J_{sc} dropped from 2.43 to 1.75 mA/cm^2. As a result, the PCE decreases from 0.46 to 0.34% for PEDOT:PSS and MoO_3 based devices, respectively, highlighting a more efficient hole extraction process, and overall device performance, by using the standard device architecture (glass/ITO/PEDOT:PSS/DONOR:PCBM/LiF/Al).

Open-circuit voltages were slightly lower than those obtained for other low-band gap materials.[33] Note that the difference in V_{oc} values of the BHJ solar cells based on **P(2,5-Py-V-EDOT)**:C_{71}−PCBM and **P(2,6-Py-V-EDOT)**:C_{71}−PCBM is ∼0.1 V, in agreement with the different HOMO energy levels of the polymers. The higher currents obtained by the devices based on **P(2,5-Py-V-EDOT)** correlate well with the better light harvesting of the pristine polymer film, in respect to the analogue **P(2,6-Py-V-EDOT)**, in the region of the absorption spectra between 350 and 500 nm, where $\Delta\lambda_{max}$ is 60 nm (Figure 4). In general, the current densities displayed from the entire set of BHJ solar cells were relatively low considering the optimum optical band gap of the donors. It is worth noting that the amount of absorbed photons depends not only on the onset

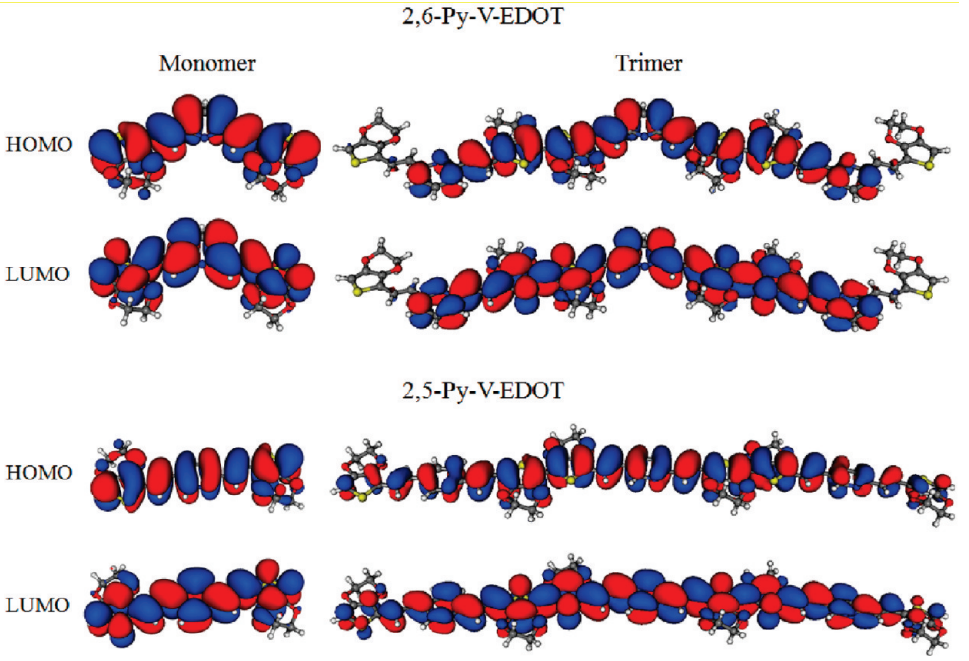

Figure 10. Isodensity plots of HOMOs and LUMOs for **2,6-Py-V-EDOT** and **2,5-Py-V-EDOT** monomers and trimers.

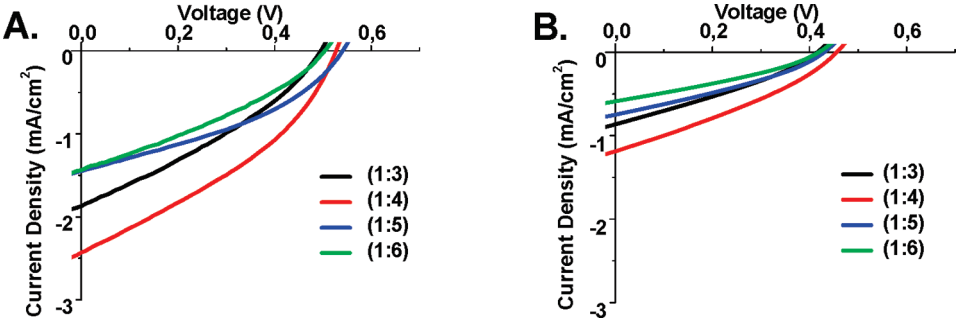

Figure 11. *J*−*V* curves under illumination of (A) **P(2,5-Py-V-EDOT)**:C_{71}−PCBM and (B) **P(2,6-Py-V-EDOT)**:C_{71}−PCBM with different weight ratios.

wavelength (E_g^{opt}) but also on the intensity of the absorption. In particular, the low absorption coefficient of the polymers, in the longer wavelength region of the spectra (> 500 nm), might contribute to the relatively low generated photocurrents. Indeed, a strong dependence of the absorption intensity, as well as other parameters such as hole mobility, optimum annealing temperature, ideal morphology, and thus ultimately OPV performance, on the molecular weight of the polymer has been recently demonstrated for P3HT.[34] We therefore believe that enhanced absorption coefficients and improved photocurrents could be achieved by increasing the molecular weight of the polymers. Moreover, longer-chain polymers could also strongly affect the nanoscale morphology of the active layer favoring exciton separation and charge transport processes with a possible improvement of the photocurrent and the fill factor. In order to optimize the light harvesting of the blend films C_{71}−PCBM was used as the acceptor, thanks to the much greater absorption in the visible region.[35] The resulting enhancement in the absorption spectra of the blends, in respect to the pristine polymers, is shown in Figure 12, where the polymer:C_{71}−PCBM blended films clearly exhibit both a broad absorption band and an improved absorption coefficient along the entire spectrum.

Table 5. Photovoltaic Parameters of the Devices Based on P(2,5-Py-V-EDOT) and P(2,6-Py-V-EDOT) with C_{71}−PCBM as the Acceptor with Various Weight Ratios

polymer	ratio[a] [wt/wt]	V_{oc} [V]	J_{sc} [mA/cm^2]	FF[b] [%]	PCE [%]
P(2,5-Py-V-EDOT)	1:3	0.50	1.87	32	0.30
	1:4	0.53	2.43	36	0.46
	1:5	0.54	1.46	37	0.29
	1:6	0.50	1.44	32	0.23
P(2,6-Py-V-EDOT)	1:3	0.42	0.87	30	0.11
	1:4	0.45	1.18	32	0.17
	1:5	0.43	0.75	31	0.10
	1:6	0.42	0.59	32	0.08

[a] Polymer:C_{71}−PCBM ratio. [b] Fill factor.

It is known that film microstructure and morphology greatly affect OPV efficiency. We investigated the morphological differences in the polymer/PCBM blend films by tapping-mode AFM. Figure 13 shows topographic images of as-cast **P(2,5-Py-V-EDOT)**:C_{71}−PCBM (1:4 wt/wt ratio) and **P(2,6-Py-V-EDOT)**:C_{71}−PCBM (1:4 wt/wt ratio) films which afforded the best OPV performance. The images reveal rms surface roughness (σ) of ∼1.11 and ∼0.74 nm for **P(2,5-Py-V-EDOT)**:C_{71}−PCBM and **P(2,5-Py-V-EDOT)**:C_{71}−PCBM films, respectively, confirming a smooth and

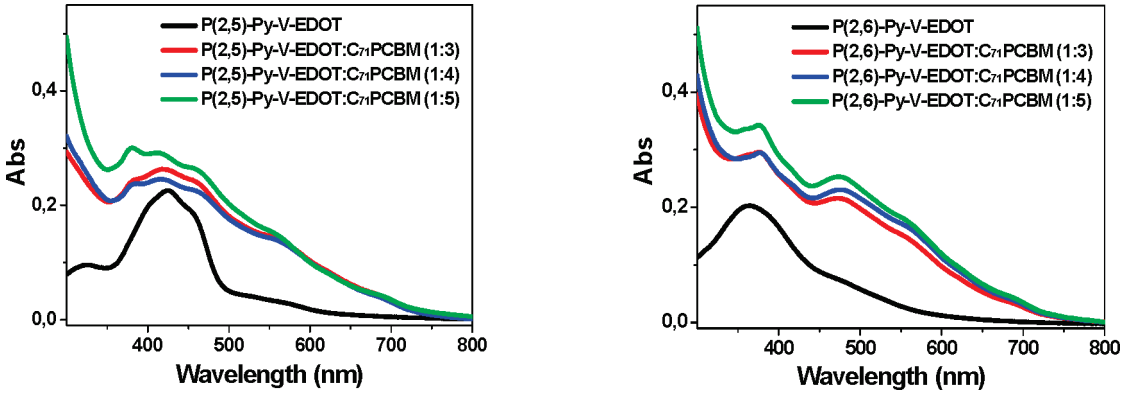

Figure 12. Absorption spectra for pristine polymers, **P(2,5-Py-V-EDOT)**:C_{71}−PCBM, and **P(2,6-Py-V-EDOT)**:C_{71}−PCBM (1:3, 1:4, and 1:5 wt/wt) thin films spin-coated from chloroform solution on glass substrates.

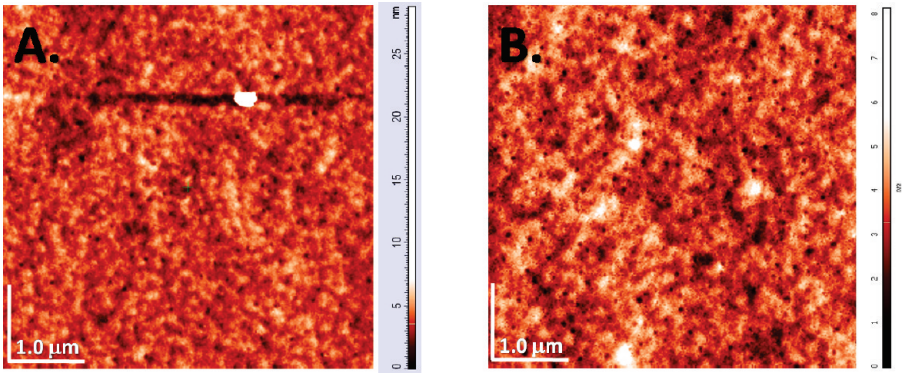

Figure 13. AFM images of as-cast **P(2,5-Py-V-EDOT)**:C_{71}−PCBM (1:4 wt/wt ratio) (left) and **P(2,6-Py-V-EDOT)**:C_{71}−PCBM (1:4 wt/wt ratio) (right) films spin-coated on glass substrates from chloroform solutions. The scan size of the images is 5 × 5 μm.

continuous surface. The thin films seem to have similar morphologies but with different domain size. In fact, the **P(2,5-Py-V-EDOT)**:C_{71}−PCBM film (Figure 13, left) exhibits smaller features with respect to the **P(2,6-Py-V-EDOT)**:C_{71}−PCBM film (Figure 13, right), which might be attributed to a more fine microstructure due to a smaller aggregation of the components. Since the morphological properties of the blends of the two polymers are similar, the observed electrical differences should then be mainly ascribed to differences on the electronic structure, HOMO−LUMO energies, and optical properties.

Hole Mobility. Hole mobility represents an important parameter for the conjugated polymer donor photovoltaic materials. Recently, it has been reported that unbalanced charge carriers mobilities, extremely low or extremely high, can contribute to losses in power conversion efficiency by a variety of mechanisms.[36] As a reference, the electron and hole mobilities of the P3HT:PCBM blend which yielded the best photovoltaic performance were in the range of 10^{-3}−10^{-4} and 10^{-4}−10^{-5} cm^2 V^{-1} s^{-1}, respectively.[37] Here we measured the hole mobility of the two polymer:C_{71}−PCBM blend films by space charge limited current (SCLC) model.[38] Hole-only devices with a structure of ITO/PEDOT:PSS/polymer:PCBM/Au were fabricated. The method for evaluating charge carrier mobility in BHJ photovoltaic cells involves fitting the experimental dark J−V curves to the Mott−Gurney equation

$$J = 9/8\mu\varepsilon\varepsilon_0 V^2/L^3$$

where J is the current density, μ is the mobility, ε is the relative permittivity of the blend (assumed to be 3), ε_0 is the permittivity of vacuum, L is the thickness of the blend layer, and V is the voltage. The effective voltage across the sample is obtained by subtracting both the built-in voltage (V_{bi}) (the difference in the work function of the anode and the cathode), and the voltage drop (V_{rs}) due to the ITO/PEDOT:PSS series resistance and contact resistance (~15 Ω) from the applied voltage. According to the Mott−Gurney equation, the hole mobilities obtained at the optimum blend composition (1:4 wt/wt for both polymers) are ~1.9×10^{-4} and ~2.1×10^{-4} cm^2 V^{-1} s^{-1} for **P(2,5-Py-V-EDOT)**:C_{71}−PCBM and **P(2,6-Py-V-EDOT)**:C_{71}−PCBM based devices, respectively. The resulting curves were plotted as $\log(J^{1/2})$ vs V, as shown in Figure S24 (Supporting Information). These results indicate an efficient hole transport across the active layer in agreement with the measured mobilities for the P3HT/PCBM blends.

It is known that reaching high charge carrier mobility and efficient light harvesting by the active materials is the general route for improving the short circuit current in a BHJ solar cell.[39] Thus, the good hole mobility obtained at the optimum blend composition of **P(2,5-Py-V-EDOT)** and **P(2,6-Py-V-EDOT)** highlight the potential of this heteroarylene−vinylene D−A−D skeleton for photovoltaic applications. In fact, we believe that polymers with higher molecular weight could yield improved PCEs by enhancing the optical absorption as well as improving electrical and morphological parameters.

Conclusion

A new class of heteroarylene−vinylene donor−acceptor−donor polymers is presented. The design has been based on the use of very simple and parent donor (EDOT) and acceptor (pyridine) heteroaromatic rings. In addition, donor and acceptor moieties have been linked through a ethenylic spacer in order to

exploit increased planarization along the π backbone and efficient π delocalization with respect to the most common approach in the literature endowed with direct aryl−aryl connection. The central pyridine acceptor core has been linked to the terminal EDOT−vinylene groups via two different substitution patterns (2,6-pyridine and 2,5-pyridine, corresponding to a *meta* cross-conjugated and a *para* conjugated pattern, respectively) in order to investigate their effects on optical and energetic properties. Indeed, the corresponding monomers showed different UV−vis, NMR, and electrochemical properties. Polymers have been prepared by both electrochemical and chemical routes. Unfortunately, the Yamamoto poly coupling route afforded low molecular weight polymers, most likely due to solubility issues associated with the unsubstituted nature of the donor/acceptor heteroaromatic fragments. As a consequence we note that the two synthetic routes did not lead exactly to the same polymers, as confirmed by the different absorption spectra (Figures 4 and 7). The presence of low-energy bands in the electrochemical polymers suggests the presence of higher molecular-weight species endowed with more extended conjugated frameworks. On the other hand the high-energy absorption profile is very similar in electrochemical and Yamamoto polymers. More importantly, the measured electrochemical bandgaps, obtained from the difference between the reduction and the oxidation potential onset (Table 3), and the optical bandgaps, calculated on the low energetic edge of the absorption spectra of the Yamamoto polymers as thin films, are identical (1.6−1.7 eV), supporting the similar nature of the species obtained by the two synthetic approaches, with the different molecular weights being the most noticeable deviation. This observation reiterates the necessity of further optimizing the polymerization conditions, in combination with more soluble donor and acceptor units, in order to achieve high molecular weight chemical polymers.

By keeping in mind this, however we note that the oxidative electropolymerization leads to polymeric films with optimal HOMO, LUMO, and low bandgap energies, in agreement with materials design rules for efficient donor polymers in OPV devices and almost identical to those of record donor polymers. These data suggest that the design based on vinylene-spaced simple donor and acceptor heteroaromatic rings could be efficiently exploited for the prepararation of new efficient materials. The relatively modest performances of BHJ photovoltaic cells here obtained for the polymers of the chemical route are mostly due to their small molecular weight. Indeed, the ideal morphology in P3HT-based OPV cells is formed when the polymer molecular weight is in the range 30 000−70 000.[2,34] Improved efficiencies are expected from these systems once new chemical routes will be envisaged for the synthesis of more soluble and higher molecular weight polymers. Studies are currently under way to build new heteroarylene−vinylene donor−acceptor polymers carrying new heteroaromatic units endowed with higher molecular weights.

Experimental Section

Materials and Methods. *Synthesis, NMR, and Optical Characterization of Monomers.* NMR spectra were recorded on a Bruker AMX-500 instrument operating at 500.13 (^{1}H) and 125.77 (^{13}C) MHz. J-MOD and 2D HSQC (heteronuclear single-quantum correlation) experiments were performed to assign ^{13}C chemical shifts. Coupling constants are given in Hz. High resolution mass spectra (HRMS) were recorded using a Bruker Daltonics ICR-FTMS APEX II spectrometer equipped with an electrospray ionization (ESI) source. Flash chromatography was performed with Merck grade 9385 silica gel 230−400 mesh (60 Å). Reactions were carried out under nitrogen in oven-dried glassware and monitored by thin layer chromatography using UV light (254 and 365 nm) as a visualizing agent. All reagents were obtained from commercial suppliers at the highest purity grade and used without further purification, except for $POCl_3$ which was distilled and *N*-bromosuccinimide (NBS) which was recrystallized prior to use. Anhydrous solvents were purchased from Sigma-Aldrich and used without further purification. Extracts were dried over Na_2SO_4 and filtered before removal of the solvent by evaporation. Melting points are uncorrected. Absorption and emission spectra were recorded on a V-570 Jasco spectrophotomer and a FP6200 Jasco spectrofluorimeter, respectively.

Chemical Characterization of Polymers. Transition temperatures were determined by differential scanning calorimetry (DSC) using a Mettler Toledo DSC 821 instrument with a heating and cooling rate of 15 °C/min under nitrogen. Thermogravimetric analyses (TGA) were performed with a Mettler Toledo TGA/DSC STARe system at a heating rate of 10 °C/min under nitrogen. Gel permeation chromatography (GPC) analyses were recorded on a Waters 1515 separation module using polystyrene as a standard and THF as an eluant.

Electrochemical and Spectroelectrochemical Experimental Details. The electrolyte was prepared from tetrabutylammonium hexafluorophosphate ((TBA)PF_6, anhydrous, ≥99.0%, Fluka), and acetonitrile, (CH_3CN, anhydrous 99.8% Aldrich), used as received. All the chemicals and the electrolyte were stored and used in a glovebox (drybox) filled with Argon ([O_2] ≤ 1 ppm). Polymer deposition (see details below) was carried out in a three-compartment cell with a Pt flag as counter, a Ag/AgCl wire as pseudoreference, and a fluorine tin oxide (FTO) as the working electrode with an exposed area of 1 cm^2. The same cell was used for polymer characterization using the deposed layer as working electrode. The Ag/AgCl pseudoreference was calibrated before each measurement using 1 mM ferrocene (Fc) solution in the electrolyte against a glassy-carbon working electrode; the resulting $E_{1/2,Fc}$ varies between 0.3 and 0.4 V. All potentials are reported vs Fc/Fc^+. For the electrochemical measurements, a potentiostat PARSTAT2273 was used. All the electrochemical measurements were performed in the glovebox. The spectroelectrochemical measurements were performed using the same cell arrangement in a sealed optical cuvette. A Jasco V-570 UV−vis−near IR was used as spectrophotometer in the NIR/visible spectra ($1100 \geq \lambda \geq 340$ nm) under several applied potentials. The potential was applied before the spectrum acquisition for a time long enough to drive the system to a stationary state, and it was maintained during the measurements.

Computational Investigation. All the calculations have been performed with the Gaussian 03 program package.[40] A 3-21G* and 6-31G* basis set were used for geometry optimizations. A 6-31G*, 6-31+G*, and 6-311++G** basis set were used for single point energy calculations. For all calculation we used a continuum polarizable model (PCM) to describe the solvation effects.[29] For the optical properties, the computational set up was calibrated in order to reproduce the absorption maxima of the reference **2,6-Py-V-EDOT** and **2,5-Py-V-EDOT** monomers. In previous papers on similar high-conjugated systems, we found a considerable red-shift of the lowest (intense) TDDFT excitation energy, calculated by the B3LYP functional,[30a] compared to the experimental absorption maxima. This shift was as large as 0.6−0.8 eV and was related to the inaccurate description of charge-transfer excited states in highly delocalized systems.[41,42] Moreover, further red-shifts were calculated by introducing solvation effects. To overcome this limitation we used here the B3LYP functional for geometry optimizations and the MPW1K functional,[43] containing 42% of Hartree−Fock exchange, for TDDFT excitation energies.[30] The increased amount of Hartree−Fock exchanges ensures a correction of the self interaction error typical of conventional functionals and also improves the long-range exchange behavior. The MPW1K excitation energies are in much better agreement with the experimental values than B3LYP values. As far as the electrochemical properties are

concerned, we proceeded with a open-shell calculation on the cationic and anionic form of the monomer ($n = 1$) and oligomer ($n = 3$) for geometry optimization and single point energy in solvent. To determinate the $\Delta G_{ox/red}$ we needed to obtain ΔG_{solv} energy in vacuo and thermal contribution for each species involved in the ox/red process (neutral, cationic, and anionic compounds). ΔG_{solv} is obtained from the differences between the total free energy in solution and the energy in vacuo at the same geometry. For the thermal contribution, we performed a very onerous frequency calculations at 6-31G* and 3-21G* geometry, which were added to the energy in vacuo at different basis-set obtaining the free energy in vacuo.

Fabrication and Characterization of Polymer Photovoltaic Cells. The polymer photovoltaic devices consisted of a thin film of a polymer blend **P(2,5-Py-V-EDOT)** or **P(2,6-Py-V-EDOT)** with C_{71}−PCBM, sandwiched in-between a transparent anode (indium tin-oxide, ITO) and a metal cathode (LiF, Al). Before device fabrication, the glass substrates coated with ITO (R_s, 4−8 Ω) were cleaned sequentially by ultrasonic treatment in detergent, deionized water, acetone, and isopropyl alcohol. At the end of the cleaning procedure the substrates were dried with nitrogen gas and placed in an oxygen plasma chamber for 10 min. A poly(3,4-ethylenedioxythiophene)/poly(styrenesulfonate) (**PEDOT:PSS**) (Baytron P) layer of about 100 nm thick was spin-coated at 2000 rpm (120 s) from an aqueous solution onto ITO coated glass substrates, followed by baking at 120 °C for 1 h. Alternatively, a MoO_3 interlayer was thermally evaporated on the precleaned ITO substrate at $\sim 10^{-6}$ Torr. The **P(2,5-Py-V-EDOT)**:C_{71}−PCBM and **P(2,6-Py-V-EDOT)**:C_{71}−PCBM solutions were prepared in dry chloroform at various polymer:PCBM weight ratios (solution concentration: 16 mg/mL). The mixture solution was then stirred for several hours at 40 °C and then spin-coated at 6000 rpm (30 s) on top of the baked **PEDOT:PSS** layer. The thickness of the polymer/C_{71}−PCBM blends is ∼80 nm. To complete the device fabrication, in the glovebox, LiF/Al (0.6 nm/70 nm) cathodes were next deposited sequentially without breaking vacuum, with a chamber pressure of $\sim 10^{-6}$ Torr. The active area of the device was approximately 6 mm^2. The current−voltage ($I-V$) characteristics were recorded by a Keithley 236 source-measure unit in the dark (for hole-only devices) and under simulated AM 1.5G irradiation (100 mW/cm^2) using a xenon lamp based solar simulator (Abet Technologies Sun 2000 Solar Simulator). All devices were tested in oxygen and moisture free nitrogen environment inside a glovebox (< 0.1 ppm of O_2 and H_2O). The thicknesses of the various films were measured by a profilometer. Atomic force microscopy (AFM) images were taken with a Solver Pro (NT-MDT) scanning probe microscope in tapping mode. Absorption of thin films was measured using a JASCO spectrometer.

Synthesis of Monomers and Polymers. *2,6-Bis[2-(3,4-ethylenedioxythien-2-yl)-ethen-1yl]pyridine* (*2,6-Py-V-EDOT*). Tetraethyl 2,6-bis(methanephosphonate)pyridine (**1**)[22] (0.36 g, 0.94 mmol), 3,4-ethylenedioxythiophene-2-carbaldehyde[23] (0.322 g, 1.88 mmol), and *t*-BuOK (0.226 g, 2.00 mmol) were dissolved in 20 mL of anhydrous THF under a nitrogen atmosphere. The reaction mixture was stirred overnight at room temperature and was poured into ice cold water (50 mL). After adding AcOEt (25 mL) the organic layer was separated, washed with brine (2 × 20 mL), dried, and evaporated to dryness to leave a yellow-orange oil which was washed with Et_2O to give the product as a yellow solid (0.290 g, 0.705 mmol, 75%): mp 136−137 °C (EtOH); λ_{max} (DMSO) = 334 nm (ε = 38000 ± 600 mol^{-1} L cm^{-1}); ^{1}H NMR (DMSO-d_6) δ 7.68 (d, 2H, J = 15.8), 7.67 (t, 1H, J = 7.8), 7.30 (d, 2H, J = 7.7), 6.89 (d, 2H, J = 15.8), 6.66 (s, 2H), 4.38−4.34 (m, 4H), 4.28−4.25 (m, 4H); ^{13}C NMR (DMSO-d_6) δ 154.45 (C), 141.99 (C), 140.69 (C), 137.38 (CH), 124.91 (CH), 121.57 (CH), 120.43 (CH), 115.17 (C), 99.71 (CH), 64.88 (CH_2), 64.37 (CH_2). HRMS-ESI m/z: calcd for $[M + H]^+$ 412.06718, found 412.06807; calcd for $[M + Na]^+$ 434.04912, found 434.04995.

2,6-Bis[2-(5-bromo-3,4-ethylenedioxythien-2-yl)-ethen-1yl]pyridine (*3*). NBS (0.250 g, 1.405 mmol) was added in one portion to a solution of 2,6-bis[2-(3,4-ethylenedioxythien-2-yl)-ethen-1yl]pyridine (**2,6-Py-V-EDOT**) (0.290 g, 0.704 mmol) in DMF (30 mL) previously cooled to −5 °C. The reaction mixture was allowed to warm gradually to room temperature. After overnight stirring, the mixture was poured into cold water (50 mL). Collection of the formed precipitate yielded the product as a brown solid with (0.320 g, 0.562 mmol, 80%), mp = 230 °C (Et_2O); ^{1}H NMR (DMSO-d_6) δ 7.68 (t, 1H, J = 15.8), 7.63 (d, 2H, J = 15.8), 7.32 (d, 2H, J = 7.7), 6.85 (d, 2H, J = 15.8), 4.42−4.37 (m, 4H), 4.36−4.32 (m, 4H); ^{13}C NMR (DMSO-d_6) δ 154.65 (C), 141.20 (C), 140.53 (C), 137.99 (CH), 125.91 (CH), 121.16 (CH), 120.04 (CH), 115.97 (C), 86.88 (C), 65.41 (CH_2), 65.35 (CH_2). HRMS-ESI m/z: calcd for $C_{21}H_{16}{}^{79}Br_2NO_4S_2[M + H]^+$ 567.88820, found 567.88871 (47%); calcd for $C_{21}H_{16}{}^{79}Br^{81}BrNO_4S_2$ $[M + H]^+$ 569.88615, found 569.88652 (100%); calcd for $C_{21}H_{16}{}^{81}Br_2NO_4S_2$ $[M + H]^+$ 571.88410, found 571.88455 (50%).

Tetraethyl 2,5-Bis(methanephosphonate)pyridine (*2*). 2,5-Bis(bromomethyl)pyridine[24] (900 mg, 3.40 mmol) was dissolved in triethylphosphite (8 mL) and the resulting mixture was refluxed for 3 h. The solvent was distilled under reduced pressure and the resulting residue was isolated as a colorless oil by flash column chromatography (silica gel, AcOEt/MeOH 8:2) (1.18 g, 3.12 mmol, 91%); ^{1}H NMR ($CDCl_3$) δ 8.45 (s, 1H), 7.64 (d, 1H, J = 8.0), 7.35 (d, 1H, J = 8.0), 4.20−3.95 (m, 8H), 3.40 (d, 2H, J = 20.8), 3.10 (d, 2H, J = 20.8), 1.25 (t, 12H, J = 7.0).

2,5-Bis[2-(3,4-ethylenedioxythien-2-yl)-ethen-1yl]pyridine (*2,5-Py-V-EDOT*). *t*-BuOK (0.785 g, 7.00 mmol) was added to a solution of tetraethyl 2,5-bis(methanephosphonate)pyridine (**2**) (1.30 g, 3.34 mmol) and 3,4-ethylenedioxythiophene-2-carbaldehyde[23] (1.16 g, 6.82 mmol) in anhyd THF (30 mL) under a nitrogen atmosphere at 0 °C. The mixture was stirred overnight at room temperature. Ethyl acetate (20 mL) and water (100 mL) were added and the formed yellow precipitate was collected as the pure product (0.650 g, 1.58 mmol, 46%): mp 201−203 °C (dec). A further amount of product was obtained by separating the organic layer, which was washed with brine (3 × 30 mL), dried, and the solvent evaporated under reduced pressure to leave the raw product (0.250 g), which is then purified by flash column chromatography (silica gel, petroleum benzene/ethyl acetate 2:8); λ_{max} (DMSO) = 410 nm (ε = 85700 ± 1700 mol^{-1} L cm^{-1}); ^{1}H NMR (CD_2Cl_2) δ 8.59 (d, 1H, J = 2.1), 7.78 (dd, 1H, J = 8.2, 1.5), 7.71 (d, 1H, J = 15.8), 7.31 (d, 1H, J = 8.2), 7.23 (d, 1H, J = 16.2), 6.97 (d, 1H, J = 15.8), 6.87 (d, 1H, J = 16.2), 6.35 (s, 1H), 6.31 (s, 1H), 4.37−4.32 (m, 4H), 4.29−4.25 (m, 4H); ^{13}C NMR (CD_2Cl_2) δ 153.83 (C), 147.77 (CH), 142.39 (C), 142.36 (C), 140.91 (C), 140.14 (C), 132.58 (CH), 131.39 (C), 124.20 (CH), 122.31 (CH), 122.15 (CH), 121.83 (CH), 119.55 (CH), 116.66 (C), 116.56 (C), 99.37 (CH), 98.57 (CH), 65.17 (CH_2), 64.93 (CH_2). HRMS-ESI m/z: calcd for $[M + H]^+$ 412.06718, found 412.06740; calcd for $[M + Na]^+$ 434.04912, found 434.04949.

2,5-Bis[2-(5-bromo-3,4-ethylenedioxythien-2-yl)-ethen-1yl]pyridine (*4*). NBS (0.215 g, 1.208 mmol) was added in one portion to a solution of 2,5-bis[2-(3,4-ethylenedioxythien-2-yl)ethen-1yl]pyridine (**2,5-Py-V-EDOT**) (0.250 g, 0.608 mmol) in DMF (30 mL) previously cooled to −5 °C. The reaction mixture was allowed to warm gradually to room temperature. After stirring overnight the mixture was poured into cold water (50 mL) to give a precipitate, which was collected affording the product as a yellow solid (0.276 g, 0.485 mmol, 80%), mp = 238 °C (Et_2O); unfortunately, even by trying several runs a side-product (ca. 10%) was always present in the final product; the mixture was used without further purification in the next polymerization step; ^{1}H NMR (DMSO-d_6, 100 °C) δ 8.62 (d, 1H, J = 1.6), 7.86 (dd, 1H, J = 8.2, 2.2), 7.57 (d, 1H, J = 15.8), 7.39 (d, 1H, J = 8.2), 7.19 (d, 1H, J = 16.2), 6.86 (d, 1H, J = 14.6), 6.83 (d, 1H, J = 15.7), 4.40 - 4.30 (m, 8H); ^{13}C NMR (DMSO-d_6, 100 °C) δ 152.99 (C), 147.40 (CH), 140.37 (C), 140.30 (C), 139.46 (C), 138.75 (C), 132.14 (CH), 130.43 (C), 125.03 (CH), 122.56 (CH), 121.21 (CH), 120.07 (CH), 118.19 (CH), 115.73 (C), 115.46 (C), 85.58 (C), 84.90 (C), 64.48 (2 CH_2), 64.39 (CH_2), 64.33 (CH_2). HRMS-ESI m/z: calcd for $C_{21}H_{16}{}^{79}Br_2NO_4S_2[M + H]^+$ 567.88820, found 567.88853 (44%); calcd for $C_{21}H_{16}{}^{79}Br^{81}BrNO_4S_2$ $[M + H]^+$

569.88615, found 569.88637 (100%); calcd for $C_{21}H_{16}{}^{81}Br_2NO_4S_2$ $[M + H]^+$ 571.88410, found 571.88418 (50%).

P(2,6-Py-V-EDOT) via Yamamoto Coupling. A solution of 2,6-bis[2-(5-bromo-3,4-ethylenedioxythien-2-yl)-ethen-1yl]pyridine (**3**) (0.500 g, 0.88 mmol) in anhydrous DMF (25 mL) was bubbled with argon for 30 min and then heated to 60 °C. A solution of bis-(1,5-cyclooctadiene)nickel(0) ($Ni(COD)_2$) (0.304 g, 1.10 mmol), 2,2′-bipyridine (0.175 g, 1.124 mmol), and freshly degassed 1,5-cyclooctadiene (0.110 mL, 0.895 mmol) in DMF (9 mL) was stirred at 60 °C for 30 min and then added to the monomer solution dropwise via cannula. The reaction mixture was stirred at 60 °C for 72 h, cooled to room temperature, and poured into ice-cold MeOH (300 mL). The formed precipitate was collected by filtration into a Soxhlet thimble and extracted with MeOH for 24 h, *n*-hexane for 24 h, and finally $CHCl_3$ for 24 h. The $CHCl_3$ fraction was washed with hot 0.01 M EDTA solution (25 mL) (pH = 3−4), hot 0.01 M EDTA solution (25 mL) (pH = 8−9), and water (50 mL). The solid was then dried under vacuum to give the polymer (0.121 g, 0.30 mmol, 34%) as a dark brown solid.

P(2,5-Py-V-EDOT) via Yamamoto Coupling. A solution of 2,5-bis[2-(5-bromo-3,4-ethylenedioxythien-2-yl)-ethen-1yl]pyridine (**4**) (1.00 g, 1.76 mmol) in anhyd DMF (50 mL) was bubbled with argon for 30 min and then heated to 60 °C. A solution of bis-(1,5-cyclooctadiene)nickel(0) ($Ni(COD)_2$) (0.608 g, 2.20 mmol), 2,2′-bipyridine (0.350 g, 2.248 mmol), and freshly degassed 1,5-cyclooctadiene (0.220 mL, 1.79 mmol) in DMF (18 mL) was stirred at 60 °C for 30 min and then added to the monomer solution dropwise via cannula. The reaction mixture was stirred at 60 °C for 24 h, cooled to room temperature, and poured into ice-cold MeOH (600 mL). The formed precipitate was collected by filtration into a Soxhlet thimble and extracted with MeOH for 24 h, *n*-hexane for 24 h, and finally $CHCl_3$ for 24 h. A very dark brown solid (0.300 g), not soluble in any solvent, was recovered from thimble. The $CHCl_3$ fraction was washed with hot 0.01 M EDTA solution (50 mL) (pH = 3−4), hot 0.01 M EDTA solution (50 mL) (pH = 8−9), and water (110 mL). The solid was then dried under vacuum to give the polymer (0.257 g, 0.63 mmol, 36%) as a dark brown solid.

2,6-Bis{2-[3,4-(2,2-dihexylpropylenedioxy)thien-2-yl]-ethen-1yl}-pyridine (*2,6-Py-V-ProDOT*). Tetraethyl 2,6-bis(methanephosphonate)pyridine[22] (0.113 g, 0.30 mmol), 3,4-(2,2-dihexylpropylenedioxy)thiophene-2-carbaldehyde[9a] (0.200 g, 0.57 mmol), and *t*-BuOK (0.081 g, 0.72 mmol) were dissolved in anhyd THF (10 mL) under a nitrogen atmosphere. The reaction mixture was stirred overnight at room temperature, then was poured into ice cold water (20 mL) and Et_2O (15 mL) was added. The organic layer was separated, washed with brine (2 × 10 mL), dried, and evaporated under reduced pressure to leave the practically pure product as a yellow oil (0.146 g, 0.19 mmol, 66%); ^{1}H NMR ($CDCl_3$) δ 7.71 (d, 2H, J = 16.0), 7.54 (t, 1H, J = 7.9), 7.19 (d, 2H, J = 7.5), 6.89 (d, 2H, J = 16.0), 6.37 (s, 2H), 3.96 (s, 4H), 3.87 (s, 4H), 1.45−1.36 (m, 8H), 1.35−1.20 (m, 32H), 0.94−0.84 (m, 12H); ^{13}C NMR ($CDCl_3$) δ 155.53 (C), 149.88 (C), 148.00 (C), 136.50 (CH), 125.62 (CH), 122.77 (CH), 120.97 (C), 119.33 (CH), 103.44 (CH), 77.74 (CH_2), 77.56 (CH_2), 43.77 (C), 31.96 (CH_2), 31.73 (CH_2), 30.13 (CH_2), 22.79 (CH_2), 22.64 (CH_2), 14.06 (CH_3). HRMS-ESI m/z: calcd for $[M + H]^+$ 776.47463, found 776.47445; calcd for $[M + Na]^+$ 798.45657, found 798.45585.

Electrochemical Synthesis of Polymers. Thin films of **P(2,6-Py-V-EDOT)** and **P(2,5-Py-V-EDOT)** were made on FTO by electrochemical polymerization. The monomers were dissolved to have a concentration of 1 mM, respectively, in the supporting electrolyte. Monomers **2,6-Py-V-EDOT** and **2,5-Py-V-EDOT** were investigated also by Cyclic Voltammetry (CV) at 50 mV s^{-1} in order to determine polymerization potential and currents (see Supporting Information). Chronopotentiometry under Galvanostatic (GS) conditions was used for the formation of the polymer films suitable for characterization; the deposition conditions were 0.1 mA cm^{-2} and 7 mC cm^{-2}. After deposition the films were washed with a large amount of the electrolyte to remove any trace of the residual monomers. Following previously reported data,[8d] the films were not allowed to dry. Layers made following the aforementioned protocol gave stable electrochemical response in CV scans. Thicker films (up to 25 mC cm^{-2}) were also produced having both higher CV current densities and better electrochromic response, although properties were unstable after a few redox cycles.

Acknowledgment. We thank Fondazione Cariplo (Grant 2007-5085) and EU through the project Marie Curie "Bio-Inspired Molecular Opto-Electronics" (EU-FP6-Marie Curie-035859 (BIMORE)) for financial support. The authors also thank Dr. Roberto Zamboni and Dr. Giampiero Ruani for helpful discussions and suggestions. F.D.A. and E.M. wish to thank Fondazione Istituto Italiano di Tecnologia, Project SEED-2009 "HELYOS", for financial support.

Supporting Information Available: Figures showing NMR spectra and cyclic voltammetry plots, tables of computational data (geometry parameters, oxidation and reduction potentials) of monomers and polymers, figures showing HOMOs and LUMOs isodensity plots and energy values and $\log(J_{1/2})$ vs V plots for polymer films, and a table of photovoltaic parameters using MoO_3 as hole-transporting interfacial layer. This material is available free of charge via the Internet at http://pubs.acs.org.

References and Notes

(1) Forrest, S. R.; Thompson, M. E. *Chem. Rev*. **2007**, *107*, 923–925.
(2) For recent reviews see: (a) Gunes, S.; Neugebauer, H.; Sariciftci, N. S. *Chem. Rev*. **2007**, *107*, 1324–1338. (b) Dennler, G.; Scharber, M. C.; Brabec, C. J. *Adv. Mater*. **2009**, *21*, 1323–1338. (c) Cheng, Y.-J.; Yang, S.-H.; Hsu, C.-S. *Chem. Rev*. **2009**, *109*, 5868–5923. (d) Chen, J.; Cao, Y. *Acc. Chem. Res*. **2009**, *42*, 1709–1718. (e) Po, R.; Maggini, M.; Camaioni, N. *J. Phys. Chem. C* **2010**, *114*, 695–706.
(3) (a) Brabec, C. J.; Sariciftci, N. S.; Hummelen, J. C. *Adv. Funct. Mater*. **2001**, *11*, 15–26. (b) Winder, C.; Sariciftci, N. S. *J. Mater. Chem*. **2004**, *14*, 1077–1086. (c) Soci, C.; Hwang, I.-W.; Moses, D.; Zhu, Z.; Waller, D.; Gaudiana, R.; Brabec, C.; Heeger, A. J. *Adv. Funct. Mater*. **2007**, *17*, 632–636. (d) Peet, J.; Kim, J. Y.; Coates, N. E.; Ma, W. L.; Moses, D.; Heeger, A. J.; Bazan, G. C. *Nat. Mater*. **2007**, *6*, 497–500. (e) Zhang, F.; Bijleveld, J.; Perzon, E.; Tvingstedt, K.; Barrau, S.; Inganas, O.; Andersson, M. R. *J. Mater. Chem*. **2008**, *18*, 5468–5474. (f) Lu, J.; Liang, F.; Drolet, N.; Ding, J.; Tao, Y.; Movileanu, R. *Chem. Commun*. **2008**, *42*, 5315–5317. (g) Hou, J.; Chen, H.-Y.; Zhang, S.; Li, G.; Yang, Y. *J. Am. Chem. Soc*. **2008**, *130*, 16144–16145. (h) Chen, C.-P.; Chan, S.-H.; Chao, T.-C.; Ting, C.; Ko, B.-T. *J. Am. Chem. Soc*. **2008**, *130*, 12828–12833. (i) Blouin, N.; Michaud, A.; Gendron, D.; Wakim, S.; Blair, E.; Neagu-Plesu, R.; Belletete, M.; Durocher, G.; Tao, Y.; Leclerc, M. *J. Am. Chem. Soc*. **2008**, *130*, 732–742. (j) Moule, A. J.; Tsami, A.; Bunnagel, T. W.; Forster, M.; Kronenberg, N. M.; Scharber, M.; Koppe, M.; Morana, M.; Brabec, C. J.; Meerholz, K.; Scherf, U. *Chem. Mater*. **2008**, *20*, 4045–4050. (k) Dante, M.; Garcia, A.; Nguyen, T.-Q. *J. Phys. Chem. C* **2009**, *113*, 1596–1600. (l) Zoombelt, A. P.; Fonrodona, M.; Wienk, M. M.; Sieval, A. B.; Hummelen, J. C.; Janssen, R. A. J. *Org. Lett*. **2009**, *11*, 903–906.
(4) For a recent review see: Beaujuge, P. M.; Reynolds, J. R. *Chem. Rev*. **2010**, *110*, 268–320.
(5) (a) Hou, J.; Zhang, S.; Chen, T. L.; Yang, Y. *Chem. Commun*. **2008**, *45*, 6034–6036. (b) Cihaner, A.; Algi, F. *Adv. Funct. Mater*. **2008**, *18*, 3583–3589. (c) Beaujuge, P. M.; Ellinger, S.; Reynolds, J. R. *Nat. Mater*. **2008**, *7*, 795–799.
(6) (a) Meijer, E. J.; De Leeuw, D. M.; Setayesh, S.; van Veenendaal, E.; Huisman, B.-H.; Blom, P. W. M.; Hummelen, J. C.; Scherf, U.; Klapwijk, T. M. *Nat. Mater*. **2003**, *2*, 678–682. (b) Mamada, M.; Nishida, J.-i.; Kumaki, D.; Tokito, S.; Yamashita, Y. *Chem. Mater*. **2007**, *19*, 5404–5409. (c) Zhang, M.; Tsao, H. N.; Pisula, W.; Yang, C.; Mishra, A. K.; Mullen, K. *J. Am. Chem. Soc*. **2007**, *129*, 3472–3473. (d) Farinola, G. M.; Babudri, F.; Cardone, A.; Omar, O. H.; Naso, F. *Pure Appl. Chem*. **2008**, *80*, 1735–1746.
(7) Havinga, E. E.; Hoeve, W.; Wynberg, H. *Polymer Bull*. **1992**, *29*, 119–126.
(8) (a) Yamamoto, T.; Zhou, Z.-h.; Kanbara, T.; Shimura, M.; Kizu, K.; Maruyama, T.; Nakamura, Y.; Fukuda, T.; Lee, B.-L.; Ooba, N.; Tomaru, S.; Kurihara, T.; Kaino, T.; Kubota, K.; Sasaki, S. *J. Am. Chem. Soc*. **1996**, *118*, 10389–10399. (b) Irvin, D. J.; DuBois, C. J. J.; Reynolds, J. R. *Chem. Commun*. **1999**, *20*, 2121–2122. (c) DuBois, C. J.; Reynolds, J. R. *Adv. Mater*. **2002**, *14*, 1844–1846.

(d) DuBois, C. J.; Abboud, K. A.; Reynolds, J. R. *J. Phys. Chem. B* **2004**, *108*, 8550–8557. (e) Thompson, B. C.; Madrigal, L. G.; Pinto, M. R.; Kang, T.-S.; Schanze, K. S.; Reynolds, J. R. *J. Polym. Sci., Part A* **2005**, *43*, 1417–1431. (f) Jung, Y. K.; Lee, J.; Lee, S. K.; Cho, H.-J.; Shim, H.-K. *J. Polym. Sci., Part A* **2006**, *44*, 4611–4620. (g) Chevallier, F.; Charlot, M.; Katan, C.; Mongin, F.; Blanchard-Desce, M. *Chem. Commun.* **2009**, *6*, 692–694.

(9) (a) Thompson, B. C.; Kim, Y.-G.; McCarley, T. D.; Reynolds, J. R. *J. Am. Chem. Soc.* **2006**, *128*, 12714–12725. (b) Galand, E. M.; Kim, Y.-G.; Mwaura, J. K.; Jones, A. G.; McCarley, T. D.; Shrotriya, V.; Yang, Y.; Reynolds, J. R. *Macromolecules* **2006**, *39*, 9132–9142. (c) Colladet, K.; Fourier, S.; Cleij, T. J.; Lutsen, L.; Gelan, J.; Vanderzande, D.; Nguyen, L. H.; Neugebauer, H.; Sariciftci, S.; Aguirre, A.; Janssen, G.; Goovaerts, E. *Macromolecules* **2007**, *40*, 65–72. (d) Mei, J.; Heston, N. C.; Vasilyeva, S. V.; Reynolds, J. R. *Macromolecules* **2009**, *42*, 1482–1487. (e) Beaujuge, P. M.; Vasilyeva, S. V.; Ellinger, S.; McCarley, T. D.; Reynolds, J. R. *Macromolecules* **2009**, *42*, 3694–3706. (f) Liu, B.; Najari, A.; Pan, C.; Leclerc, M.; Xiao, D.; Zou, Y. *Macromol. Rapid Commun.* **2010**, *31*, 391–398.

(10) (a) Zotti, G.; Zecchin, S.; Schiavon, G.; Berlin, A.; Penso, M. *Chem. Mater.* **1999**, *11*, 3342–3351. (b) Zotti, G.; Zecchin, S.; Schiavon, G.; Berlin, A. *J. Electroanal. Chem.* **2001**, *506*, 106–114. (c) Gadisa, A.; Mammo, W.; Andersson, L. . .M.; Admassie, S.; Zhang, F.; Andersson, M. .R.; Inganäs, O. *Adv. Funct. Mater.* **2007**, *17*, 3836–3842. (d) Pang, H.; Skabara, P. J.; Crouch, D. J.; Duffy, W.; Heeney, M.; McCulloch, I.; Coles, S. J.; Horton, P. N.; Hursthouse, M. B. *Macromolecules* **2007**, *40*, 6585–6593. (e) Balan, A.; Gunbas, G.; Durmus, A.; Toppare, L. *Chem. Mater.* **2008**, *20*, 7510–7513. (f) Beaujuge, P. M.; Ellinger, S.; Reynolds, J. R. *Adv. Mater.* **2008**, *20*, 2772–2776. (g) Cihaner, A.; Algi, F. *Adv. Funct. Mater.* **2008**, *18*, 3583–3589. (h) Gunbas, G. E.; Durmus, A.; Toppare, L. *Adv. Mater.* **2008**, *20*, 691–695. (i) Hou, J.; Zhang, S.; Chen, T. L.; Yang, Y. *Chem. Commun.* **2008**, *45*, 6034–6036. (j) Kulkarni, A. P.; Zhu, Y.; Babel, A.; Wu, P.-T.; Jenekhe, S. A. *Chem. Mater.* **2008**, *20*, 4212–4223. (k) Zhu, Y.; Kulkarni, A. P.; Wu, P.-T.; Jenekhe, S. A. *Chem. Mater.* **2008**, *20*, 4200–4211. (l) Beaujuge, P. M.; Ellinger, S.; Reynolds, J. R. *Nat. Mater.* **2008**, *7*, 795–799. (m) Barlow, S.; Bredas, J.-L.; Kippelen, B.; Marder, S. R.; Reynolds, J. R. *J. Am. Chem. Soc.* **2009**, *131*, 2824–2826. (n) Tsai, J.-H.; Chueh, C.-C.; Lai, M.-H.; Wang, C.-F.; Chen, W.-C.; Ko, B.-T.; Ting, C. *Macromolecules* **2009**, *42*, 1897–1905. (o) Zhou, H.; Yang, L.; Stoneking, S.; You, W. *ACS Appl. Mater. Interfaces* **2010**, *2*, 1377–1383.

(11) Roncali, J. *Chem. Rev.* **1997**, *97*, 173–206.

(12) Groenendaal, L.; Zotti, G.; Aubert, P.-H.; Waybright, S. M.; Reynolds, J. R. *Adv. Mater.* **2003**, *15*, 855–879.

(13) *Comprehensive Heterocyclic Chemistry*; Katritzky, A. R., Rees, C. W., Eds.; Pergamon Press: Oxford, U.K., 1984.

(14) (a) Abbotto, A.; Bradamante, S.; Pagani, G. A. *J. Org. Chem.* **1993**, *58*, 444–448. (b) Abbotto, A.; Bradamante, S.; Pagani, G. A.; Rzepa, H.; Stoppa, F. *Heterocycles* **1995**, *40*, 757–776. (c) Bradamante, S.; Pagani, G. A. *Pure And Appl. Chem.* **1989**, *61*, 709–716. (d) Bradamante, S.; Pagani, G. A. Benzyl and Heteroarylmethyl Carbanions: Structure and Substituents Effects. In *Advances In Carbanion Chemistry*; Snieckus, V., Ed.; Jai Press: Tokyo, 1996; pp 189−263.

(15) Burland, D. M.; Miller, R. D.; Walsh, C. A. *Chem. Rev.* **1994**, *94*, 31–75.

(16) He, G. S.; Tan, L.-S.; Zheng, Q.; Prasad, P. N. *Chem. Rev.* **2008**, *108*, 1245–1330.

(17) (a) Blatchford, J. W.; Jessen, S. W.; Lin, L.-B.; Gustafson, T. L.; Fu, D.-K.; Wang, H.-L.; Swager, T. M.; MacDiarmid, A. G.; Epstein, A. J. *Phys. Rev. B* **1996**, *54*, 9180–9189. (b) Epstein, A. J.; Blatchford, J. W.; Wang, Y. Z.; Jessen, S. W.; Gebler, D. D.; Gustafson, T. L.; Lin, L. B.; Wang, H.-L.; Park, Y. W.; Swager, T. M.; MacDiarmid, A. G. *Synth. Met.* **1996**, *78*, 253–261.

(18) Thompson, B.; Fréchet, J.M. .J. *Angew. Chem., Int. Ed.* **2008**, *47*, 58–77.

(19) Scharber, M. .; Mühlbacher, D.; Koppe, M.; Denk, P.; Waldauf, C.; Heeger, A. .J.; Brabec, C. .J. *Adv. Mater.* **2006**, *18*, 789–794.

(20) Chen, H.-Y.; Hou, J.; Zhang, S.; Liang, Y.; Yang, G.; Yang, Y.; Yu, L.; Wu, Y.; Li, G. *Nat. Photonics* **2009**, *3*, 649–653.

(21) Liang, Y.; Xu, Z.; Xia, J.; Tsai, S.-T.; Wu, Y.; Li, G.; Ray, C.; Yu, L. *Adv. Mater.* **2010**, *22*, E135–E138.

(22) Reppy, M. A.; Cooper, M. E.; Smithers, J. L.; Gin, D. L. *J. Org. Chem.* **1999**, *64*, 4191–4195.

(23) Raimundo, J.-M.; Blanchard, P.; Gallego-Planas, N.; Mercier, N.; Ledoux-Rak, I.; Hierle, R.; Roncali, J. *J. Org. Chem.* **2002**, *67*, 205–218.

(24) Wörsdörfer, U.; Vögtle, F.; Nieger, M.; Waletzke, M.; Grimme, S.; Glorius, F.; Pfaltz, A. *Synthesis* **1999**, *4*, 597–602.

(25) Warr, R. J.; Willis, A. C.; Wild, S. B. *Inorg. Chem.* **2006**, *45*, 8618–8627.

(26) (a) Grenier, C. R. G.; George, S. J.; Joncheray, T. J.; Meijer, E. W.; Reynolds, J. R. *J. Am. Chem. Soc.* **2007**, *129*, 10694–10699. (b) Walczak, R. M.; Cowart, J. S.; Reynolds, J. R. *J. Mater. Chem.* **2007**, *17*, 254–260.

(27) Leriche, P.; Turbiez, M.; Monroche, V.; Frère, P.; Blanchard, P.; Skabara, P. J.; Roncali, J. *Tetrahedron Lett.* **2003**, *44*, 649–652.

(28) Zhang, X.; Steckler, T. T.; Dasari, R. R.; Ohira, S.; Potscavage, W. J.; Tiwari, S. P.; Coppée, S.; Ellinger, S.; Barlow, S.; Brédas, J.-L.; Kippelen, B.; Reynolds, J. R.; Marder, S. R. *J. Mater. Chem.* **2010**, *20*, 123.

(29) (a) Becke, A. D. *J. Chem. Phys.* **1993**, *98*, 5648–5652. (b) Cossi, M.; Barone, V. *J. Chem. Phys.* **2001**, *115*, 4708–4717.

(30) (a) Pastore, M.; Mosconi, E.; De Angelis, F.; Grätzel, M. *J. Phys. Chem. C* **2010**, *114*, 7205. (b) Abbotto, A.; Manfredi, N.; Marinzi, C.; Angelis, F. D.; Mosconi, E.; Yum, J.-H.; Xianxi, Z.; Nazeeruddin, M. K.; Gratzel, M. *Energy Environ. Sci.* **2009**, *2*, 1094–1101.

(31) Karsten, B. P.; Bijleveld, J. C.; Viani, L.; Cornil, J.; Gierschner, J.; Janssen, R. A. J. *J. Mater. Chem.* **2009**, *19*, 5343.

(32) (a) Irwin, M. D.; Buchholz, D. B.; Hains, A. W.; Chang, R. P. H.; Marks, T. J. *Proc. Natl. Acad. Sci. U.S.A.* **2008**, *105*, 2783. (b) Vishal, S.; Gang, L.; Yan, Y.; Chih-Wei, C.; Yang, Y. *Appl. Phys. Lett.* **2006**, *88*, 073508. (c) Zhang, F.; Sun, F.; Shi, Y.; Zhuo, Z.; Lu, L.; Zhao, D.; Xu, Z.; Wang, Y. *Energy Fuels* **2010**, *24*, 3739–3742. (d) Yamanari, T.; Taima, T.; Sakai, J.; Tsukamoto, J.; Yoshida, Y. *Jpn. J. Appl. Phys.* **2010**, *49*, 01AC02.

(33) (a) Wang, X.; Perzon, E.; Mammo, W.; Oswald, F.; Admassie, S.; Persson, N.-K.; Langa, F.; Andersson, M. R.; Inganas, O. *Thin Solid Films* **2006**, *511−512*, 576–580. (b) Martijn, M. W.; Mathieu, G. R. T.; Martin, P. S.; Marta, F.; Rene, A. J. J. *Appl. Phys. Lett.* **2006**, *88*, 153511.

(34) (a) Schilinsky, P.; Asawapirom, U.; Scherf, U.; Biele, M.; Brabec, C. J. *Chem. Mater.* **2005**, *17*, 2175–2180. (b) Ma, W.; Kim, J. Y.; Lee, K.; Heeger, A. J. *Macromol. Rapid Commun.* **2007**, *28*, 1776–1780. (c) Ballantyne, A. M.; Chen, L.; Dane, J.; Hammant, T.; Braun, F. M.; Heeney, M.; Duffy, W.; McCulloch, I.; Bradley, D. D. C.; Nelson, J. *Adv. Funct. Mater.* **2008**, *18*, 2373–2380. (d) Muller, C.; Wang, E.; Andersson, L. M.; Tvingstedt, K.; Zhou, Y.; Andersson, M. R.; Inganas, O. *Adv. Funct. Mater.* **2010**, *20*, 2124–2131.

(35) (a) Arbogast, J. W.; Foote, C. S. *J. Am. Chem. Soc.* **1991**, *113*, 8886. (b) Wienk, M. M.; Kroon, J. M.; Verhees, W. J. H.; Knol, J.; Hummelen, J. C.; Van Hal, P. A.; Janssen, R. A. J. *Angew. Chem., Int. Ed.* **2003**, *42*, 3371.

(36) Mandoc, M. M.; Koster, J. J. A.; Blom, P. W. M. *Appl. Phys. Lett.* **2007**, *90*, 133504.

(37) Mihailetchi, V. D.; Xie, H.; de Boer, B.; Koster, J. A.; Blom, P. W. M. *Adv. Funct. Mater.* **2006**, *16*, 699.

(38) (a) Chung, D. S.; Lee, D. H.; Yang, C.; Hong, K.; Park, C. E.; Park, J. W.; Kwon, S. K. *Appl. Phys. Lett.* **2008**, *93*, 033303. (b) Blom, P. W. M.; De Jong, M. J. M.; Vleggaar, J. J. M. *Appl. Phys. Lett.* **1996**, *68*, 3308.

(39) Hoppe, H.; Sariciftci, N. S. *J. Mater. Res.* **2004**, *19*, 1924–1945.

(40) Gaussian 03, R., D., Frisch, M. J.; Trucks, G. W.; Schlegel, H. B.; Scuseria, G. E.; Robb, M. A.; Cheeseman, J. R.; Montgomery, J. A., Jr.; Vreven, T.; Kudin, K. N.; Burant, J. C.; Millam, J. M.; Iyengar, S. S.; Tomasi, J.; Barone, V.; Mennucci, B.; Cossi, M.; Scalmani, G.; Rega, N.; Petersson, G. A.; Nakatsuji, H.; Hada, M.; Ehara, M.; Toyota, K.; Fukuda, R.; Hasegawa, J.; Ishida, M.; Nakajima, T.; Honda, Y.; Kitao, O.; Nakai, H.; Klene, M.; Li, X.; Knox, J. E.; Hratchian, H. P.; Cross, J. B.; Adamo, C.; Jaramillo, J.; Gomperts, R.; Stratmann, R. E.; Yazyev, O.; Austin, A. J.; Cammi, R.; Pomelli, C.; Ochterski, J. W.; Ayala, P. Y.; Morokuma, K.; Voth, G. A.; Salvador, P.; Dannenberg, J. J.; Zakrzewski, V. G.; Dapprich, S.; Daniels, A. D.; Strain, M. C.; Farkas, O.; Malick, D. K.; Rabuck, A. D.; Raghavachari, K.; Foresman, J. B.; Ortiz, J. V.; Cui, Q.; Baboul, A. G.; Clifford, S.; Cioslowski, J.; Stefanov, B. B.; Liu, G.; Liashenko, A.; Piskorz, P.; Komaromi, I.; Martin, R. L.; Fox, D. J.; Keith, T.; Al-Laham, M. A.; Peng, C. Y.; Nanayakkara, A.; Challacombe, M.; Gill, P.M. W.; Johnson, B.; Chen, W.; Wong, M. W.; Gonzalez, C.; Pople, J. A. Gaussian, Inc.: Pittsburgh PA, 2003.

(41) Hagberg, D. P.; Yum, J.-H.; Lee, H.; De Angelis, F.; Marinado, T.; Karlsson, K. M.; Humphry-Baker, R.; Sun, L.; Hagfeldt, A.; Graetzel, M.; Nazeeruddin, M. K. *J. Am. Chem. Soc.* **2008**, *130*, 6259–6266.

(42) Kim, S.; Lee, J. K.; Kang, S. O.; Ko, J.; Yum, J.-H.; Fantacci, S.; De Angelis, F.; Di Censo, D.; Nazeeruddin, M. K.; Graetzel, M. *J. Am. Chem. Soc.* **2006**, *128*, 16701–16707.

(43) Lynch, B. J.; Fast, P. L.; Harris, M.; Truhlar, D. G. *J. Chem. Phys.* **1999**, *110*, 7650.